INVESTIGATION OF A RADIALLY VIBRATING, OIL FILLED CYLINDRICAL CERAMIC TRANSDUCER WITH A VARIABLE INTERNAL IMPEDANCE AND DEVOID OF ALL FORMS OF PRESSURE RELEASE

GUY C. JARRATT

INVESTIGATION OF A RADIALLY VIBRATING, OIL FILLED CYLINDRICAL CERAMIC TRANSDUCER WITH A VARIABLE INTERNAL IMPEDANCE AND DEVOID OF ALL FORMS OF PRESSURE RELEASE

* * * * *

Guy C. Jarratt, III

INVESTIGATION OF A RADIALLY VIBRATING, OIL FILLED CYLINDRICAL CERAMIC TRANSDUCER WITH A VARIABLE INTERNAL IMPEDANCE AND DEVOID OF ALL FORMS OF PRESSURE RELEASE

by

Guy C. Jarratt, III
Lieutenant, United States Navy

Submitted in partial fulfillment of
the requirements for the degree of

MASTER OF SCIENCE
IN
ENGINEERING ELECTRONICS

United States Naval Postgraduate School
Monterey, California

1963

INVESTIGATION OF A RADIALLY VIBRATING, OIL FILLED CYLINDRICAL CERAMIC TRANSDUCER WITH A VARIABLE INTERNAL IMPEDANCE AND DEVOID OF ALL FORMS OF PRESSURE RELEASE

by

Guy C. Jarratt, III

This work is accepted as fulfilling

the thesis requirements for the degree of

MASTER OF SCIENCE

IN

ENGINEERING ELECTRONICS

from the

United States Naval Postgraduate School

ABSTRACT

A radially vibrating, oil filled, cylindrical ceramic transducer devoid of all forms of pressure release provides a means of transmitting sound at unlimited depths. A study was made of the admittance characteristics in the vicinity of resonance of a transducer of this type, which was constructed with a variable acoustic impedance in the oil filled interior. The results were compared with theoretical computations, which proved helpful in analyzing and interpreting the resonances of the transducer. Additional measurements were made on the transducer and were utilized in the computation of electroacoustic efficiency at the major resonances.

The writer wishes to express his appreciation for the assistance and encouragement given him in this investigation by Mr. Joe Martin of the Bendix-Pacific Division of North Hollywood, California.

TABLE OF CONTENTS

LIST OF ILLUSTRATIONS

LIST OF ILLUSTRATIONS

LIST OF ILLUSTRATIONS

SYMBOLS

a	Radius of ceramic (inside)
b	Radius of inner steel tube (outside)
B_E	Electrical susceptance
b_{EM}	Electromechanical susceptance
b_M	Mechanical susceptance
b_o	Clamped susceptance
C_B	Transducer capacitance far below resonance
C_{BC}	Bridge balance cable capacitance
c_E	Sound velocity of external medium
c_I	Sound velocity of internal medium
C_M	Mechanical compliance in air
c_o	Sound velocity in ceramic
C_o	Clamped capacitance
C_p	Transducer parallel capacitance
C_T	Initial bridge capacitance balance
C_{TC}	Transducer cable capacitance
d_{33}	Ceramic piezoelectric constant
d_i	Inside diameter of ceramic ring
d_m	Mean diameter of ceramic ring
d_o	Outside diameter of ceramic ring
f	Frequency
f_{AA}	Anti-resonant frequency in air

f_{RA}	Resonant frequency in air
F_C	Circumferential force of system
F_R	Radial force of system
G_E	Electrical conductance
g_{EM}	Electromechanical conductance
g_M	Mechanical conductance
g_o	Clamped conductance
h	Height of ceramic ring
j	Imaginary unit ($\sqrt{-1}$)
J_o, J_1	Bessel functions of the first kind
k	Wavelength constant ($\frac{\omega}{c}$)
k_{33}	Electromechanical coupling coefficient
K	Stiffness of ceramic
K_o	Clamped dielectric constant
KE	Kinetic energy of system
$\dot{\overline{KE}}$	Rate of change of kinetic energy
L_M	Mechanical inductance in air
M	Mass of system
M_o	Mass of ceramic
N	Number of stripes or segments for tangentially polarized cylinder
N_o, N_1	Neumann functions of the first kind
r	Specific radiation resistance

R_B	Bridge resistor
R_M	Mechanical resistance times $4\pi^2$
R_{MC}	Mechanical resistance
R_o	Clamped resistance
R_p	Transducer parallel resistance
R_R	Radiation resistance
t	Wall thickness of ceramic ring
W	Work done on system
$\dot{W}$	Rate of doing work
X_E	Specific radiation reactance of external medium
$\overline{X}_E$	External radiation reactance
X_I	Specific radiation reactance of internal medium
$\overline{X}_I$	Internal radiation reactance
$\overline{X}_{MC}$	Mechanical reactance
Y_{33}	Young's modulus of bare ceramic
Y_E	Electrical admittance
Y_{EM}	Electromechanical admittance
Y_M	Mechanical admittance
Y_o	Effective Young's Modulus of ceramic
Y_{TC}	Transducer and cable admittance
Z_E	Electrical impedance
Z_M	Mechanical impedance
Z_o	Characteristic impedance

Z_{TC}	Transducer and cable impedance
η	Electroacoustic efficiency
η_M	Mechanical efficiency
ξ_R	Radial displacement of ceramic ring
$\dot{\xi}_R$	Radial velocity of ceramic ring
$\ddot{\xi}_R$	Radial acceleration of ceramic ring
ξ_c	Circumferential displacement of ceramic ring
$\dot{\xi}_c$	Circumferential velocity of ceramic ring
$\ddot{\xi}_c$	Circumferential acceleration of ceramic ring
ρ_E	Density of external medium
ρ_I	Density of internal medium
ρ_o	Density of ceramic
ϕ^2	Electromechanical conversion factor
σ	Radiation area
ω	Angular frequency
ψ	Ratio (b/a)
Tanδ	Dissipation factor

1. Introduction.

In recent years there has developed a growing need for deep submergence transducers. Until now most of the transducers developed have utilized some form of pressure-release. The most common forms of pressure-release have been the specially developed materials "Corprene" and "Celltite" rubber, or cavities inside the transducer filled with air. These forms of pressure release are satisfactory for only limited depths of submergence. Corprene and Celltite loose their effectiveness at about a 100 foot depth, because the air in the cells of the material is lost under hydrostatic pressure. When this occurs mechanical hysteresis effects are exhibited under cyclic changes of hydrostatic pressure, impairing the acoustic properties of the transducer. The air-cavity systems can be operated to greater depths, but they too, have a depth limit set by the mechanical strength of the transducer. By utilizing compressed-air for pressure-compensation the maximum working depth of the air-cavity systems can be increased; but this method is limited by the addition of bulky equipment and failures that are usually catastrophic. The failure of pressure release systems to operate satisfactorily at great depths has revealed a pressing need for investigation of the acoustic properties of transducers devoid of all forms of pressure-release.

It has become possible to produce transducers of almost any shape desired from polarized ferroelectric ceramics such as barium titanate. As a result, increased interest has been shown in the possibilities of designing

transducers with thin-walled ceramic cylinders devoid of all forms of pressure release. Radially vibrating transducers of this type, having the interior of the cylinder constructed of two concentric oil filled cavities separated by a perforated metal tube, have been built. These transducers have proved to be successful in operating at great depths.

This paper presents an investigation of the effect of varying the area of the holes which couple the concentric oil filled cavities in a transducer of the type described above. Most of this effort will be based on experimental results obtained by a series of experiments involving a concentric stack of barium titanate cylinders with a variable percentage opening, stiff, central, tube, which presents varying impedance conditions to the inside of the oil filled, radially vibrating, ceramic cylinders. Where it is possible to do so, the results of these tests will be compared with theory in an effort to arrive at design criteria allowing prediction of frequency, impedance and efficiency.

2. Transducer Description.

The essential features of the variable internal impedance transducer, Model DX-304, are shown in Figures 2.1, 2.2, and 2.3 (see inside back cover). The active portion is composed of barium titanate ceramic cylinders on a common axis. Each cylinder is tangentially polarized and striped with alternate stripes being connected together electrically, enabling the cylinder to be driven in the radial mode. The cylinders have an average outside diameter of 6.19 inches, height of 2.875 inches and thickness of .5 inches. The oil filled interior is divided into two concentric cavities by a pair of closely fitting concentric steel tubes lying along the cylindrical axis. The combination of the slots in the tube walls and the rotatable interior tube permit the variation of the acoustic coupling between the cavities. Varying the acoustic coupling results in a variation of the impedance presented to the inside of the ceramic cylinders. The percentage of opening in the slotted tubes can be varied from 50 percent opening to zero percent opening (fully closed). A pressure equalizing line assures equal hydrostatic pressure inside and outside the acoustic array at all times. This feature permits operation at practically unlimited depths. Spacers provide isolation between each cylinder and between the acoustic array and the outer slotted tube.

Figure 2.1 . External View of the Variable Internal Impedance Transducer

Figure 2.2 Internal View of the Variable Internal Impedance Transducer

3. Equivalent Electrical Circuit of the Transducer.

Consider a ceramic cylinder of height (h), mean diameter (d_m), and wall thickness (t), which is tangentially polarized and driven in the radial mode.[1] The ratio h/d_m is made small to avoid critical coupling into the longitudinal mode.[2] The ratio t/d_m is small; therefore, the radial displacement (ξ_R) and the radial velocity ($\dot{\xi}_R$) can be considered uniform over the cylinder.[2] The radially vibrating cylinder can then be treated as a lumped mechanical system in a radial frame of reference. In order to simplify the mathematics the parameters will be established in the radial frame of reference and related to the parameters in the circumferential frame of reference, where work done by Mason[3] on thickness vibrators may be utilized.

Relating displacement in the radial and circumferential frames of reference gives:

$$\xi_c = 2\pi \xi_R \tag{3.1}$$

Expressions relating velocity and acceleration follow from Equation (3.1) by differentiation.

Expressing the kinetic energy of the system in the radial frame of reference gives:

$$KE = \tfrac{1}{2} M \dot{\xi}_R^2$$

where M is the total mass of the system and

$$\dot{\overline{KE}} = M \ddot{\xi}_R \dot{\xi}_R = F_R \dot{\xi}_R \tag{3.2}$$

where

$$F_R = M \ddot{\xi}_R$$

The work done on the system may be expressed in the circumferential frame of reference as:

$$W = F_c \xi_c$$

and

$$\dot{W} = F_c \dot{\xi}_c = 2\pi F_c \dot{\xi}_R \tag{3.3}$$

The Conservation of Energy requires[4]:

$$\dot{\overline{KE}} = \dot{W} \tag{3.4}$$

Therefore substituting Equations (3.2) and (3.3) into (3.4) gives:

$$F_R = 2\pi F_c \tag{3.5}$$

Now consider the forces acting on a radiating ceramic cylinder:

a. Force resulting from motion ($\ddot{\xi}_R$) of the ceramic:

$$F_R = M_o \ddot{\xi}_R = 2\pi F_c$$

$$\therefore F_c = \frac{M_o \ddot{\xi}_c}{4\pi^2} \tag{3.6}$$

where $M_o = \rho_o \pi d_m ht$ = mass of the ceramic.

b. Force resulting from stiffness (K) of ceramic:

$$F_c = -K \xi_c \tag{3.7}$$

where $$K = \frac{Y_o h t}{\pi d_m} = \frac{\rho_o c_o^2 h t}{\pi d_m}$$

c. Force resulting from energy radiated and energy dissipated in mechanical losses:

$$F_R = -R_M \dot{\xi}_R = 2\pi F_c$$

$$F_c = \frac{R_M \dot{\xi}_c}{4\pi^2} \tag{3.8}$$

where

$$R_M = \frac{R_R}{\eta_M} = \frac{\rho_E c_E \pi d_o h}{\eta_M}$$

d. Force resulting from motion of external medium:

$$F_R = j \mathcal{X}_E \dot{\xi}_R = 2\pi F_c$$

$$F_c = j \frac{\mathcal{X}_E \dot{\xi}_c}{4\pi^2} \tag{3.9}$$

where

$$\mathcal{X}_E = \chi_E \rho_E c_E \pi d_o h$$

e. Force resulting from motion of internal medium (neglecting viscous losses):

$$F_R = \pm j \mathcal{X}_I \dot{\xi}_R = 2\pi F_c$$

$$F_c = \pm j \frac{X_I \dot{\xi}_c}{4\pi^2} \tag{3.10}$$

where

$$X_I = X_I \rho_I c_I \pi d_i h$$

Now consider the application of a sinusodial driving force along the circumference of the ring. The result of this driving force is to maintain the ceramic ring in a condition of vibration. Writing the differential equation for the motion of the ceramic ring results in:

$$\frac{M_o}{4\pi^2}\ddot{\xi}_c + \left(j\frac{X_E}{4\pi^2} \pm j\frac{X_I}{4\pi^2} + \frac{R_M}{4\pi^2}\right)\dot{\xi}_c + K\xi_c = F_c e^{j\omega t} \tag{3.11}$$

The solution of the differential equation gives for the displacement and velocity the following:[5]

$$\xi_c = \frac{-jF e^{j\omega t}}{\omega\left[\frac{R_M}{4\pi^2} + j\left(\frac{M_o\omega}{4\pi^2} + \frac{X_E}{4\pi^2} \pm \frac{X_I}{4\pi^2} - \frac{K}{\omega}\right)\right]} \tag{3.12}$$

$$\dot{\xi}_c = \frac{F e^{j\omega t}}{\frac{R_M}{4\pi^2} + j\left(\frac{M_o\omega}{4\pi^2} + \frac{X_E}{4\pi^2} \pm \frac{X_I}{4\pi^2} - \frac{K}{\omega}\right)} \tag{3.13}$$

From Equation (3.13) the mechanical impedance (Z_M) is found to be:

$$Z_m = \frac{R_m}{4\pi^2} + j\left(\frac{M_o\omega}{4\pi^2} + \frac{X_E}{4\pi^2} \pm \frac{X_I}{4\pi^2} - \frac{K}{\omega}\right) \qquad (3.14)$$

or

$$Z_m = R_{MC} + j X_{MC}$$

where

$$R_{MC} = \frac{R_m}{4\pi^2}$$

and

$$X_{MC} = \frac{M_o\omega}{4\pi^2} + \frac{X_E}{4\pi^2} \pm \frac{X_I}{4\pi^2} - \frac{K}{\omega}$$

Mechanical resonance[5] occurs when:

$$X_{MC} = 0 \qquad (3.15)$$

In air $\bar{X}_E = \bar{X}_I = 0$; therefore,

$$X_{MC} = \frac{M_o\omega}{4\pi^2} - \frac{K}{\omega} = 0 \qquad (3.16)$$

Substituting in Equation (3.16) for the values of M_o, ω and K, and then solving for resonant frequency in air (f_{RA}) gives:

$$f_{RA} = \frac{c_o}{\pi d_m} \qquad (3.17)$$

Utilizing the relationship in Equation (3.17) and letting

$$Z_o = \rho_o c_o h t \tag{3.18}$$

the mechanical parameters are found to be:

$$R_M = \left(\frac{\pi \rho_E c_E \pi d_o}{\eta_M \rho_o c_o t} \right) Z_o \tag{3.19}$$

$$M_o = \frac{Z_o}{f_{RA}} \tag{3.20}$$

$$X_E = \left(\frac{X_E \rho_E c_E \pi d_o}{\rho_o c_o t} \right) Z_o \tag{3.21}$$

$$X_I = \left(\frac{X_I \rho_I c_I \pi d_i}{\rho_o c_o t} \right) Z_o \tag{3.22}$$

$$K = f_{RA} Z_o \tag{3.23}$$

The equivalent circuit of the radially vibrating ceramic cylinder is given in Figure 3.1,

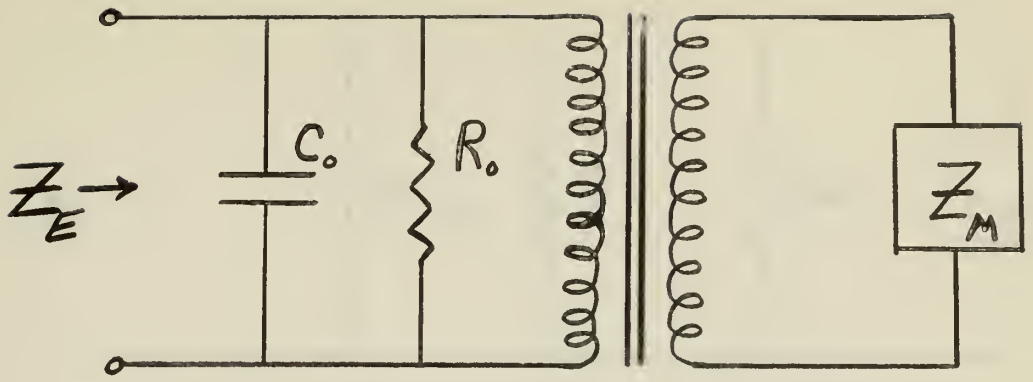

Figure 3.1 Equivalent Circuit in Terms of Impedance.

or in terms of admittance in Figure 3.2,

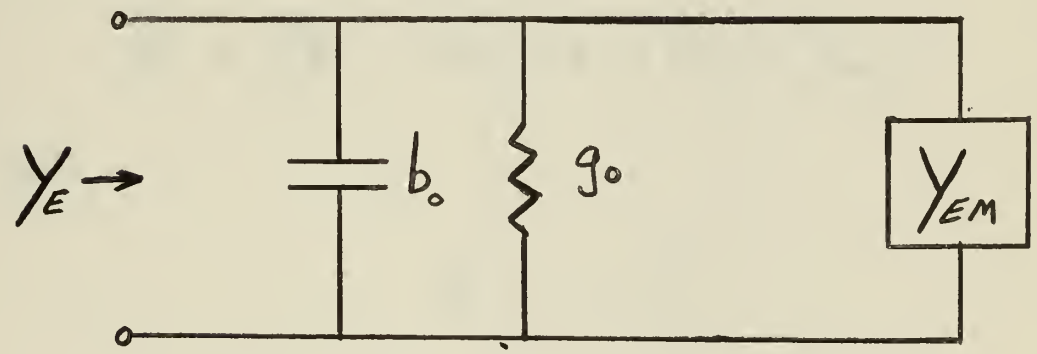

Figure 3.2 Equivalent Circuit in Terms of Admittance.

where $$Y_{EM} = \phi^2 Y_M = \frac{\phi^2}{Z_M} = \phi^2 g_M + j\phi^2 b_M$$

or $$Y_{EM} = g_{EM} + j b_{EM}$$

Thus, the equivalent circuit utilized in making theoretical computations is shown in Figure 3.3.

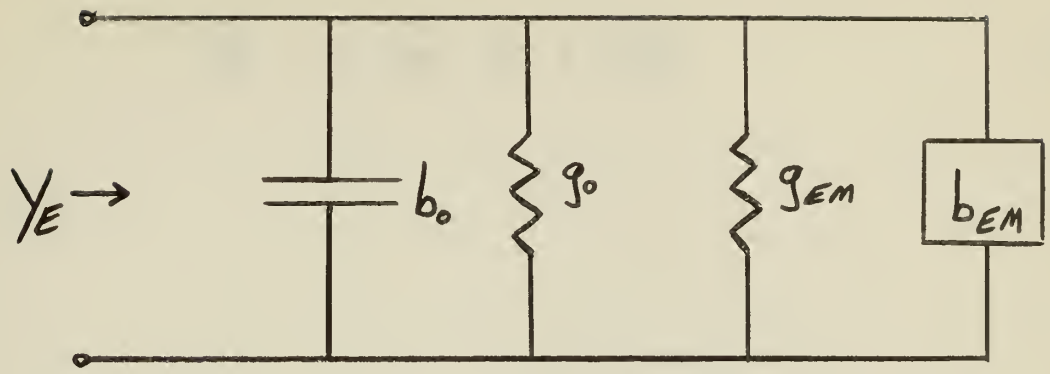

Figure 3.3 Equivalent Circuit in Terms of Parallel Equivalents.

Therefore, by definition,

$$Y_E = (g_o + g_{EM}) + j(b_o + b_{EM}) \tag{3.24}$$

where

$$b_o = \omega C_o \tag{3.25}$$

$$g_o = \frac{1}{R_o} = b_o \tan\delta \tag{3.26}$$

$$g_{EM} = \frac{\phi^2 R_{MC}}{|Z_M|^2} \tag{3.27}$$

$$b_{EM} = \frac{\phi^2 X_{MC}}{|Z_M|^2} \tag{3.28}$$

or

$$Y_E = G_E + j B_E \tag{3.29}$$

4. Measurements Procedure.

All water tests made on the variable internal impedance transducer were conducted in a fresh water test tank. The tank is made of concrete, and is 30 feet long, 18 feet wide, 13 feet deep in the middle, sloping to 16 feet at the sides. In all tests a short, 1.5 to 2.5 millisecond, pulse was used at a rate of ten pulses per second, in order that reflections in the tank would not interfere with the test results. The transducer was kept centrally located in the tank for measurements. When a calibrated hydrophone was used in conjunction with the transducer, it was placed 3 meters from the transducer and both were located centrally in the tank.

Admittance measurements were made over the frequency range of interest using the bridge circuit shown in Figure 4.1. The pulsed signal was applied to the bridge, which was then balanced. The values read on the bridge variable resistor and capacitor after balancing were equivalent to the transducer values of parallel resistance and capacitance. These values were converted to parallel values of conductance (G_E) and susceptance (B_E) of the transducer.

High power impedance measurements were made using the circuit found in Figure 4.2 with approximately 44 watts input to the transducer. The pulsed signal was amplified and applied to the transducer through a transformer. A variable inductor was placed in series with the transducer in order to reduce the phase angle. Frequency, peak-to-peak voltage, peak-to-peak current, phase angle, and the inductance of the

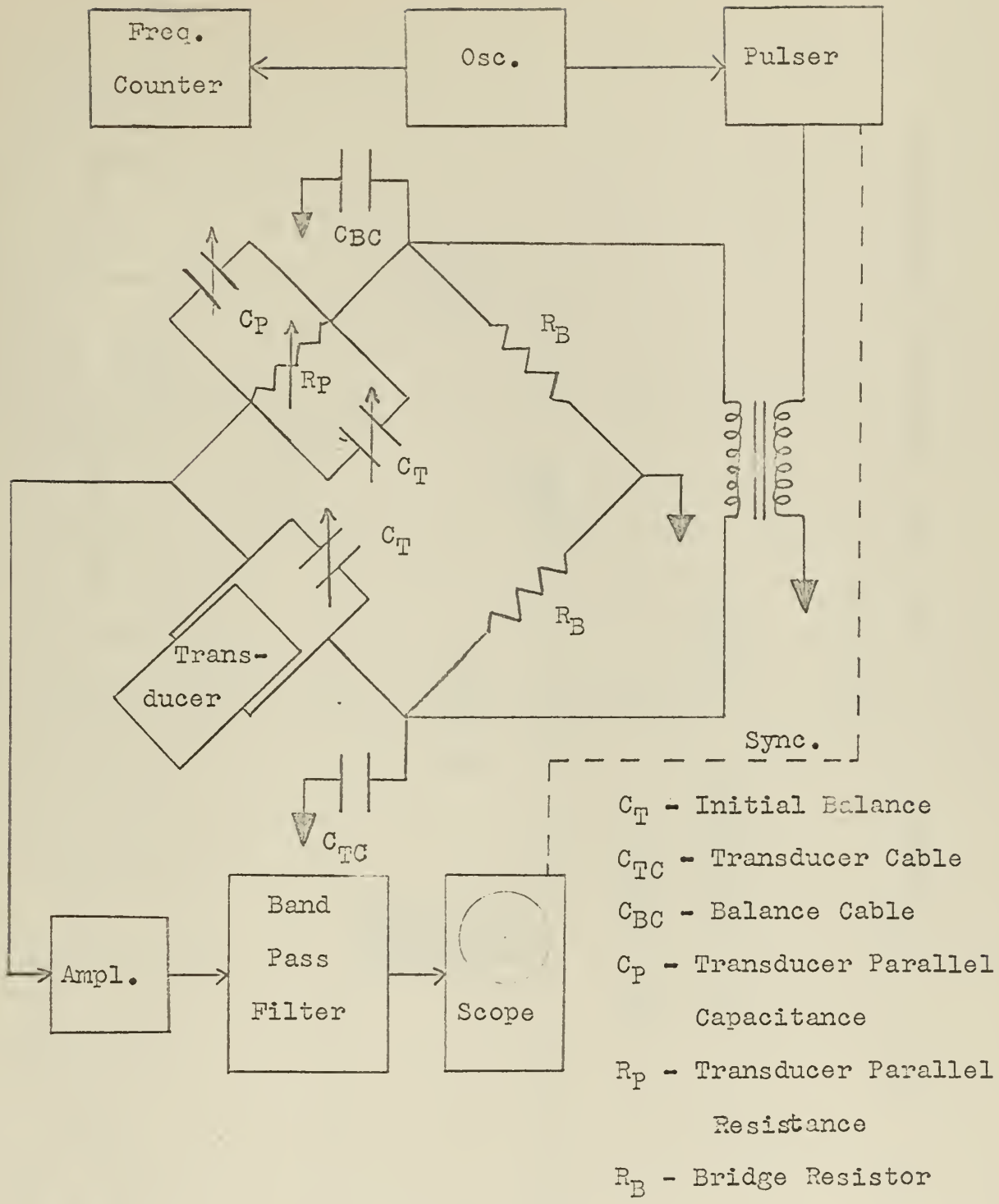

Figure 4.1

Block Diagram of Equipment Used for Transducer Admittance(G_E) and Susceptance(B_E) Measurements

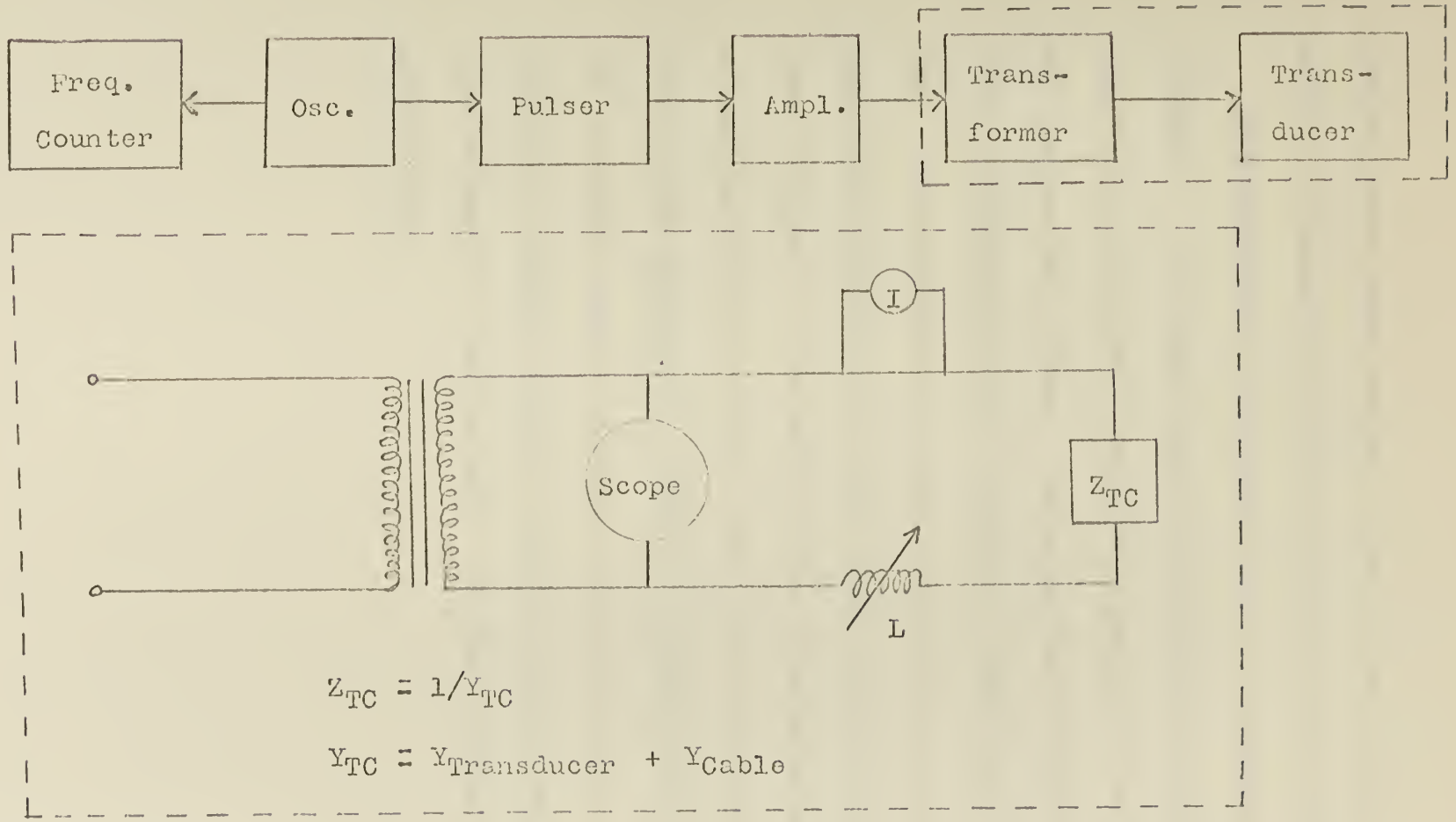

Figure 4.2

Block Diagram of Equipment Used for High Power Impedance Measurements

variable inductor were measured. From this set of data the values of parallel conductance and parallel susceptance were calculated.

The arrangement for the transmit response measurements is presented in Figure 4.3. The pulsed signal was amplified and applied to the transducer with the input current measured by means of a one ohm resistor and a vacuum tube voltmeter. The signal from the transducer was picked up by a calibrated hydrophone, amplified, filtered, and displayed on a scope. The amplitude of the signal appearing on the scope was compared with the amplitude of a known signal from the calibration circuit shown in Figure 4.3. The output voltage of the calibrated hydrophone was obtained by this procedure. Beam pattern measurements were also made with this arrangement. While the transducer was rotated through 360^{o}, the signal from the transducer was picked up by a calibrated hydrophone, amplified, filtered, amplified logarithmically, the proper signal selected by a gate and delay, and then displayed on a beam pattern recorder.

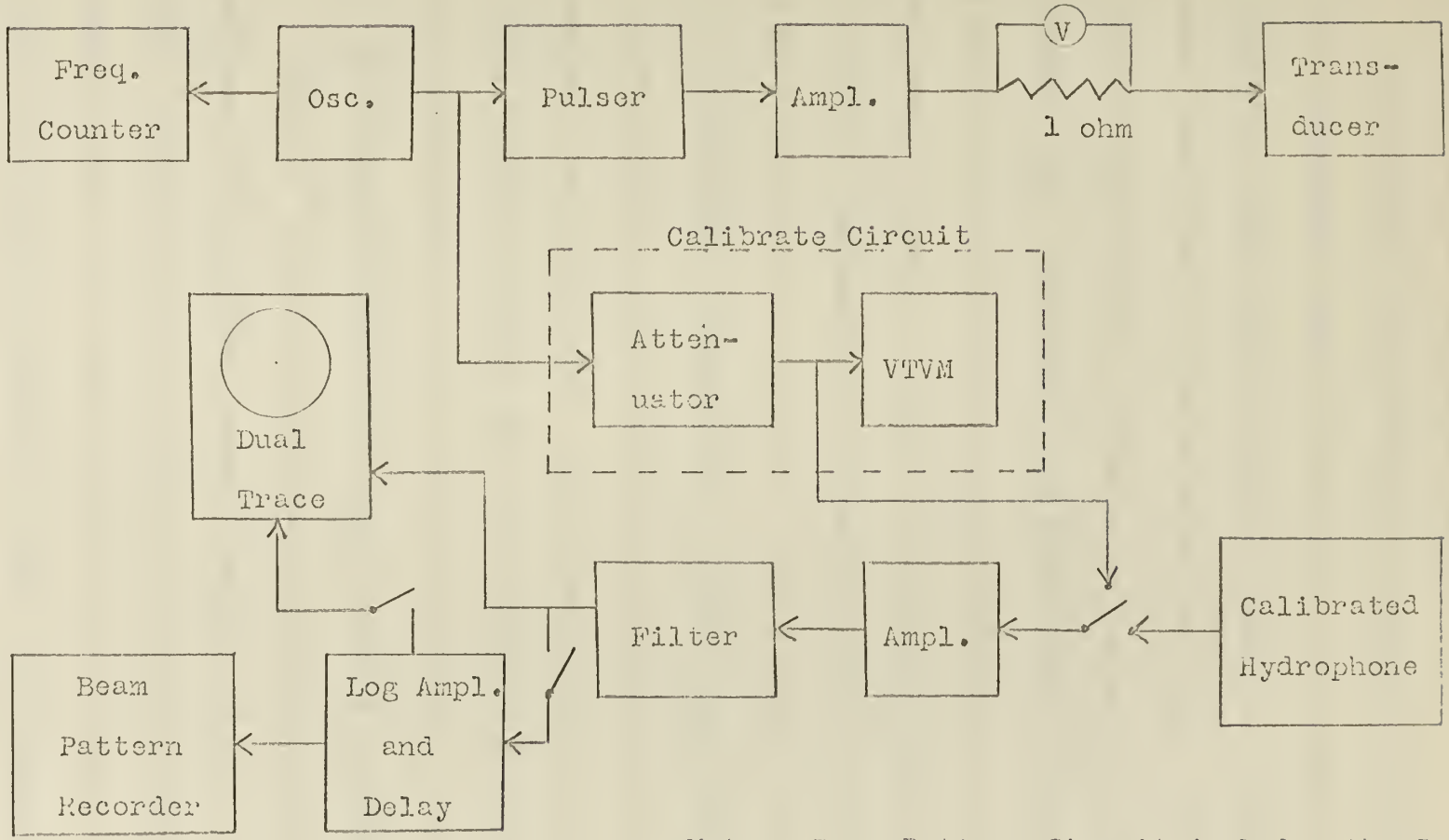

Note: Beam Pattern Circuit includes the Log Amplifier and Delay and the Beam Pattern Recorder

Figure 4.3

Block Diagram of Equipment Used for Transmit Response and Beam Patterns

5. Theoretical and Experimental Results.

The equivalent circuit developed in Section 3 was utilized in computing the theoretical curves of conductance and susceptance for the transducer in water plotted in Figures 5.1 and 5.2. The theoretical curves were plotted assuming no mechanical losses. The values of specific external radiation resistance (r) and specific external radiation reactance (X_E) were obtained from NRDC Volume 13[6] for all four figures. Two conditions of the internal acoustic impedance are considered: in one, curve A Figures 5.1 and 5.2, the interior is filled entirely with oil, which is comparable with 100 percent opening in the slotted tubes; in the second, curve B Figures 5.1 and 5.2, part of the oil is displaced by a concentrically positioned rigid cylinder, which divides the interior into two oil filled concentric cavities and compares with zero percent opening in the slotted tubes. The appropriate values of the specific internal radiation reactance (X_I) were obtained from work by Robey[7] on free flooded vibrating cylinders for the first condition. The values of X_I for the second condition were taken from work by Zilinskas.[8]

Zilinskas[8] derived an expression for the specific internal radiation reactance of a liquid filled, radially vibrating, ceramic cylinder in air with a stiff inner tube of any diameter up to the inner diameter of the ceramic cylinder. The volume between the two cylinders was considered filled with a pressure compensating liquid. The following assumptions were made:

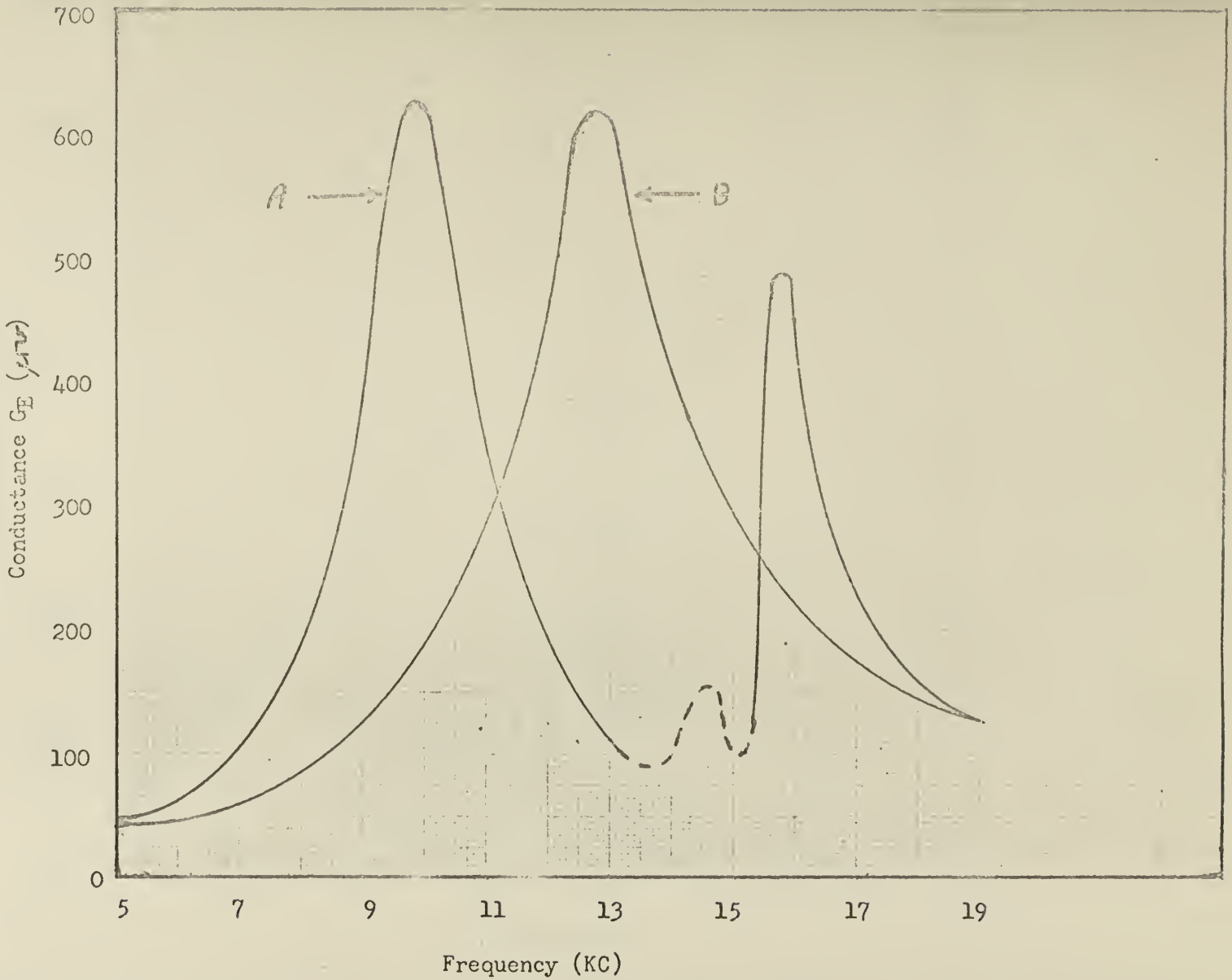

Figure 5.1 Theoretical Plots of Conductance (G_E) Versus Frequency of the Five Ring Variable Internal Impedance Transducer with and without a Stiff Inner Tube

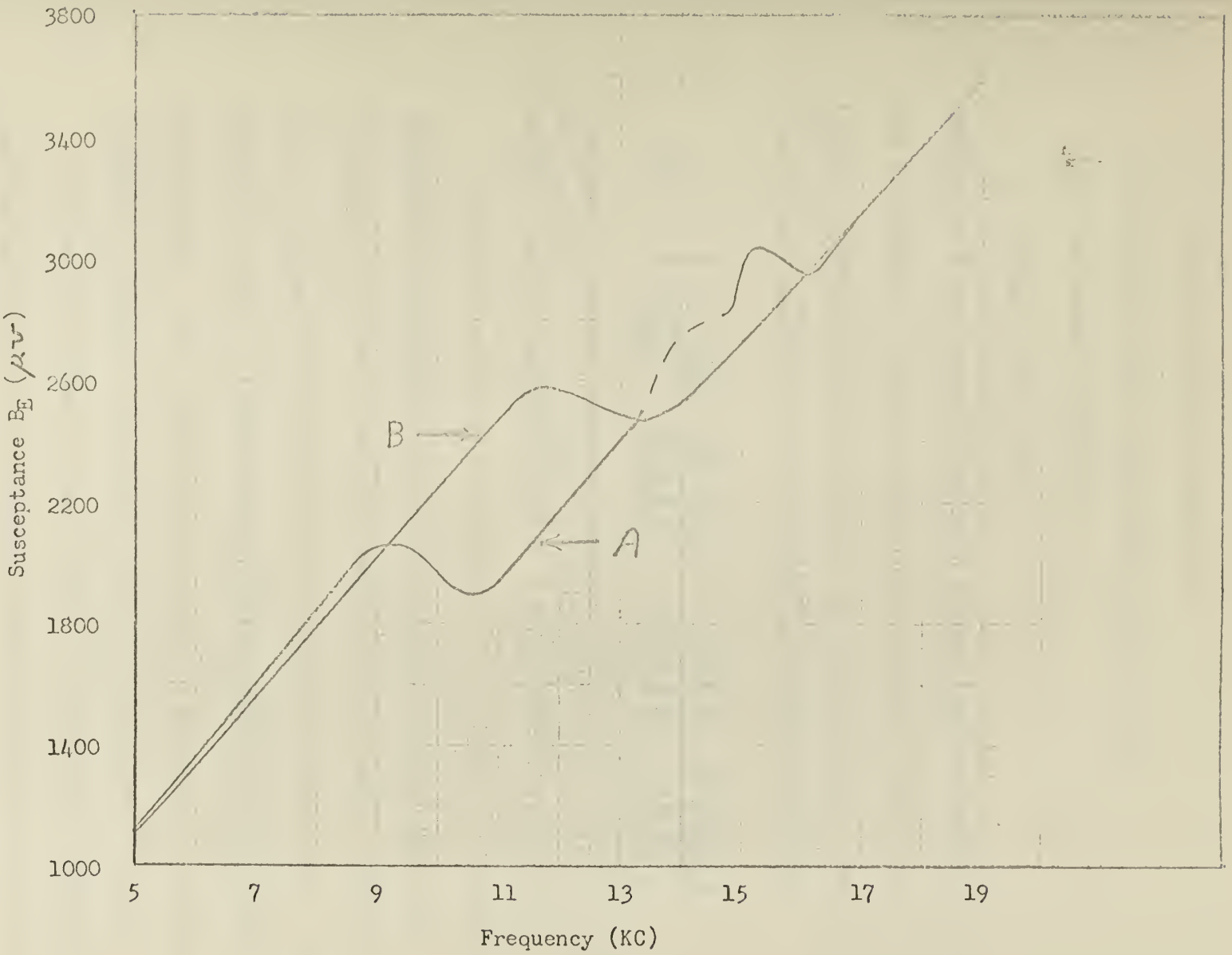

Figure 5.2 Theoretical Plots of Susceptance (B_E) Versus Frequency of the Five Ring Variable Internal Impedance Transducer with and without a Stiff Inner Tube

(1) Radially symmetric vibrations

(2) Constant radial displacement along the axis

(3) Non-viscous liquid fill

(4) Infinitely long cylinder.

Starting with the dynamical equation for the fluid and working in cylindrical coordinates, Zilinskas arrived at the following expression for the specific internal radiation reactance (X_I) of the cylinder after applying the above assumptions and the appropriate boundary conditions.

$$X_I = j \frac{J_1(kb)\, N_0(ka) - J_0(ka)\, N_1(kb)}{J_1(ka)\, N_1(kb) - J_1(kb)\, N_1(ka)}$$

The specific internal radiation reactance (X_I) of the cylinder is plotted against ka, for a parametric set of $\psi = \frac{b}{a}$ ratios, in Figure 5.3.

The graphs on Figures 5.4 through 5.7 were plotted from bridge admittance measurements made on the variable internal impedance transducer described in Section 2, while it was in water. Figures 5.4 and 5.5 represent the transducer with five barium titanate rings, while Figures 5.6 and 5.7 represent the transducer with only three barium titanate rings. Both sets of graphs reveal the effect of varying the percentage of opening in the slotted steel tubes inside the transducer.

The graph on Figure 5.8 was plotted from high power impedance measurements made on the variable internal impedance transducer described in Section 2 with five rings and zero percent opening of the slotted tubes (fully closed), while it was in water. Comparison of this curve

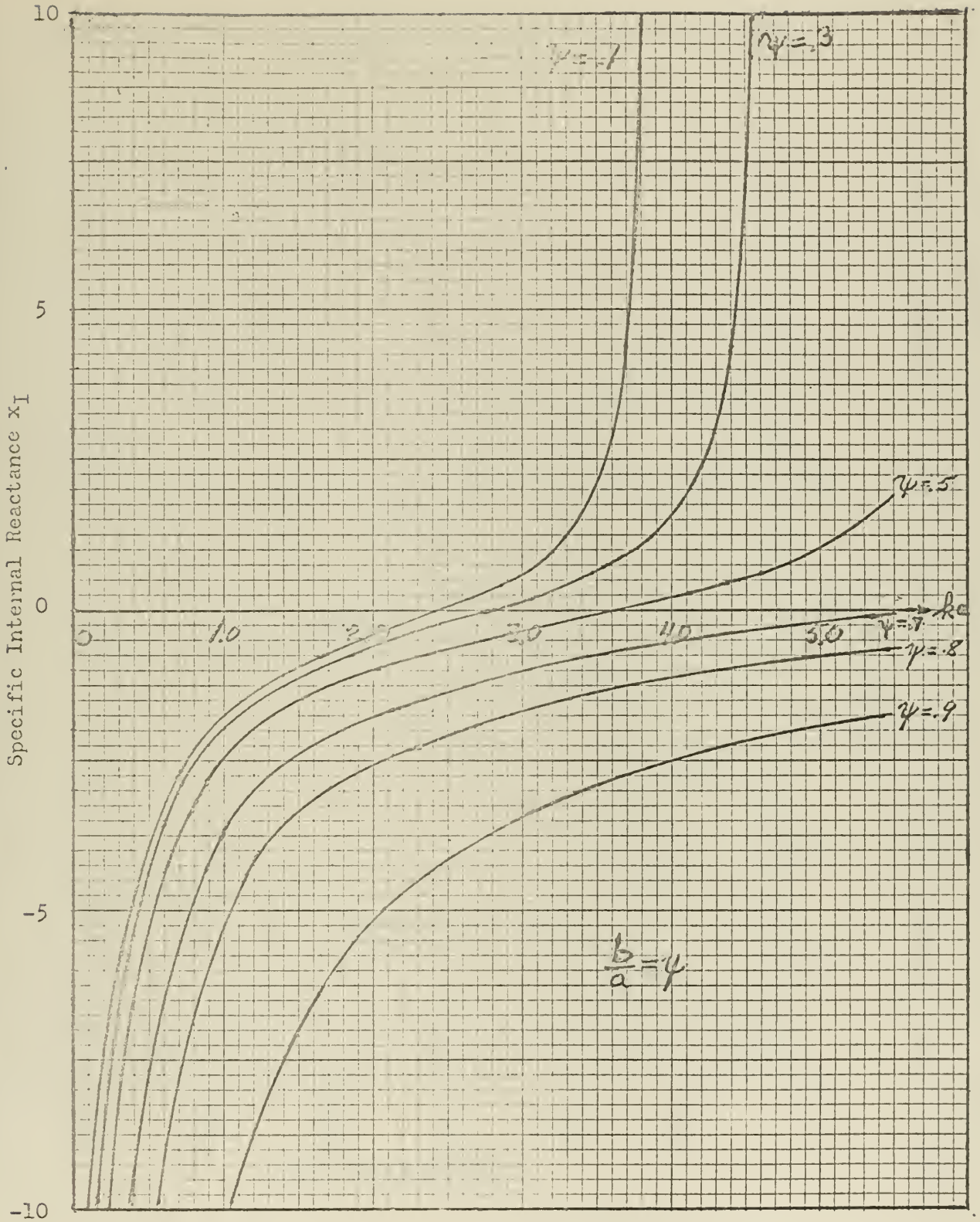

Figure 5.3 Plot of Specific Internal Radiation Reactance (x_I) of a Liquid Filled Cylinder with an Inner Concentric Stiff Tube

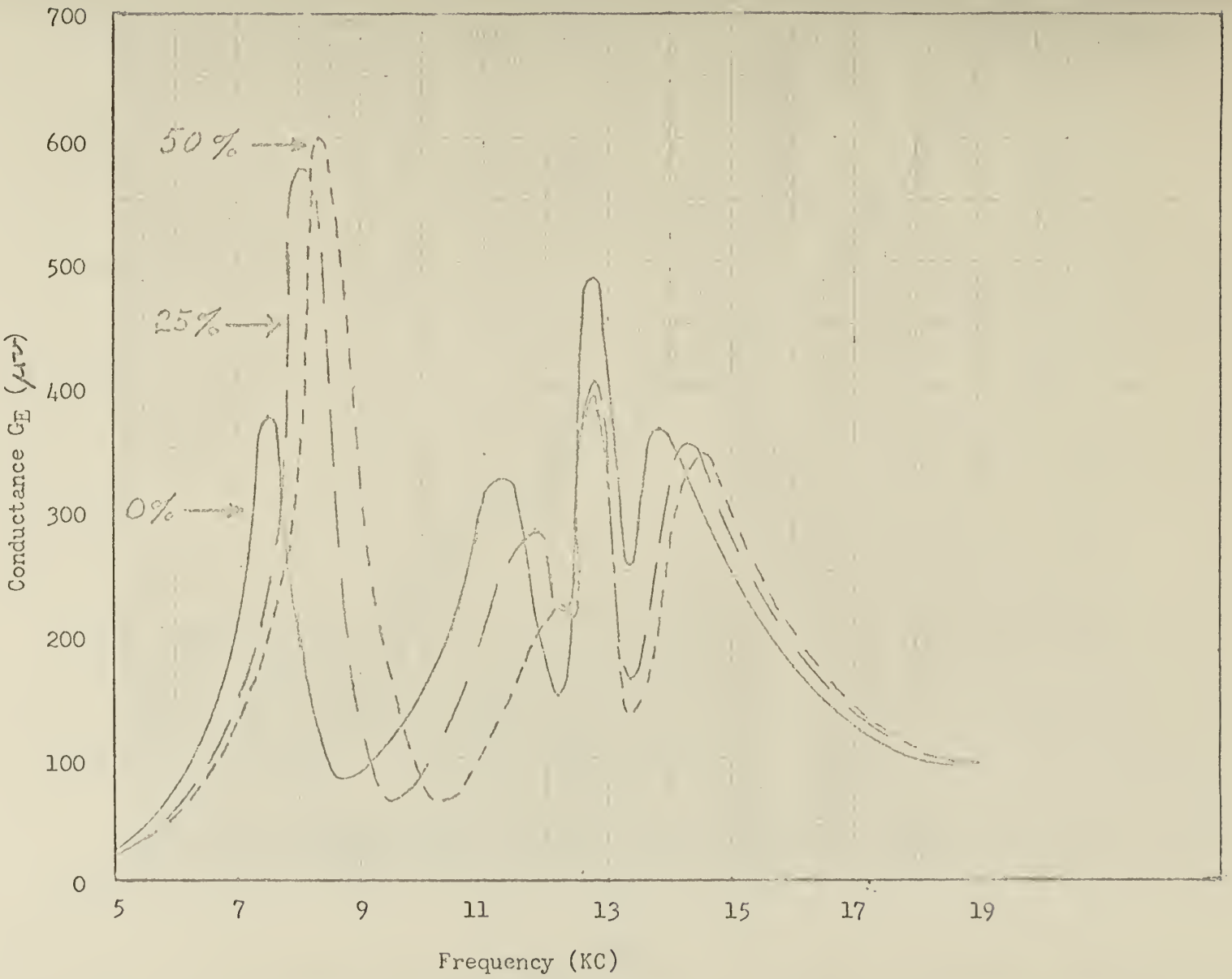

Figure 5.4 Plot of Conductance (G_E) Versus Frequency of the Five Ring Variable Internal Impedance Transducer for Three Different Settings of the Variable Impedance Tube

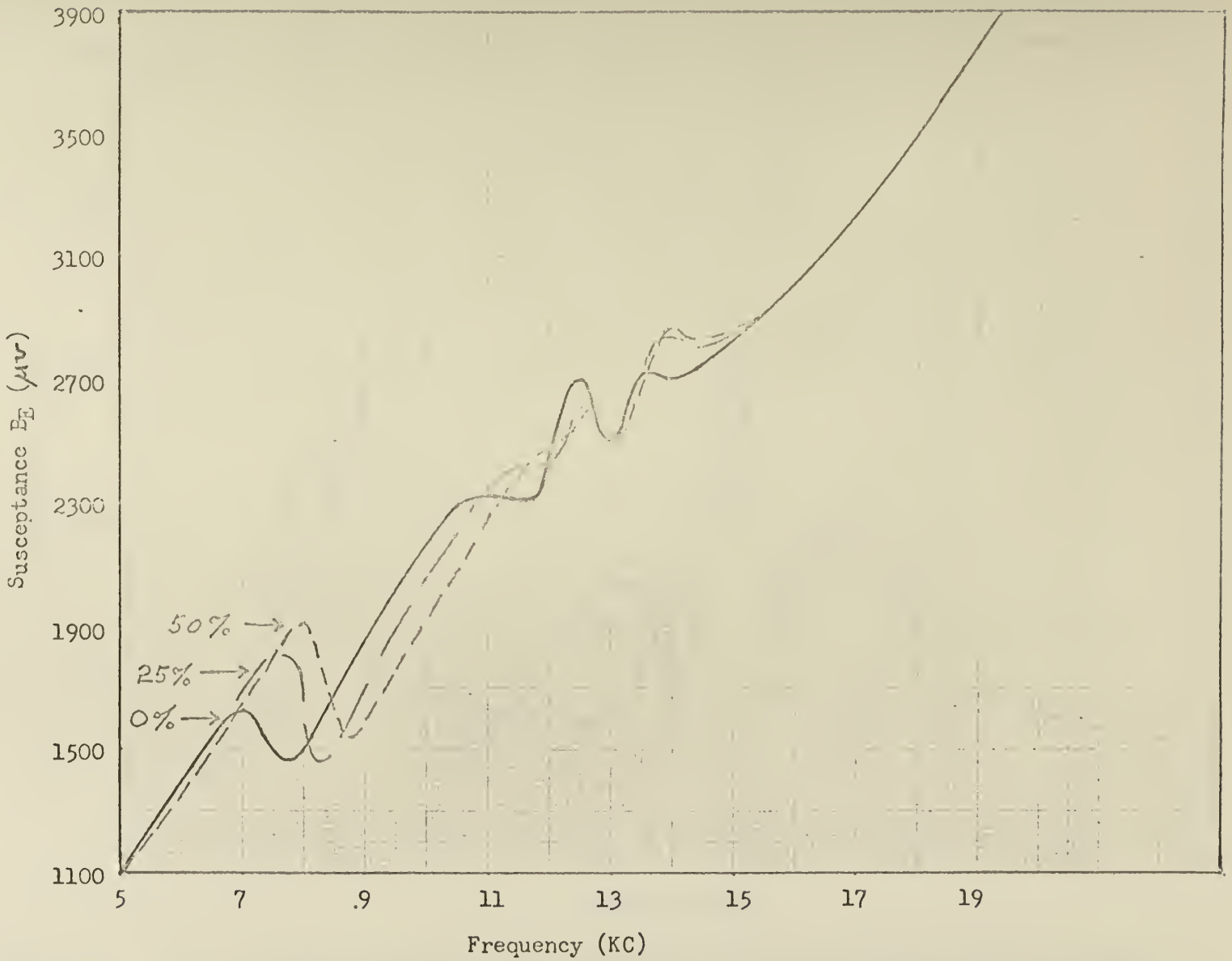

Figure 5.5 Plot of Susceptance (B_E) Versus Frequency of the Five Ring Variable Internal Impedance Transducer for Three Different Settings of the Variable Impedance Tube

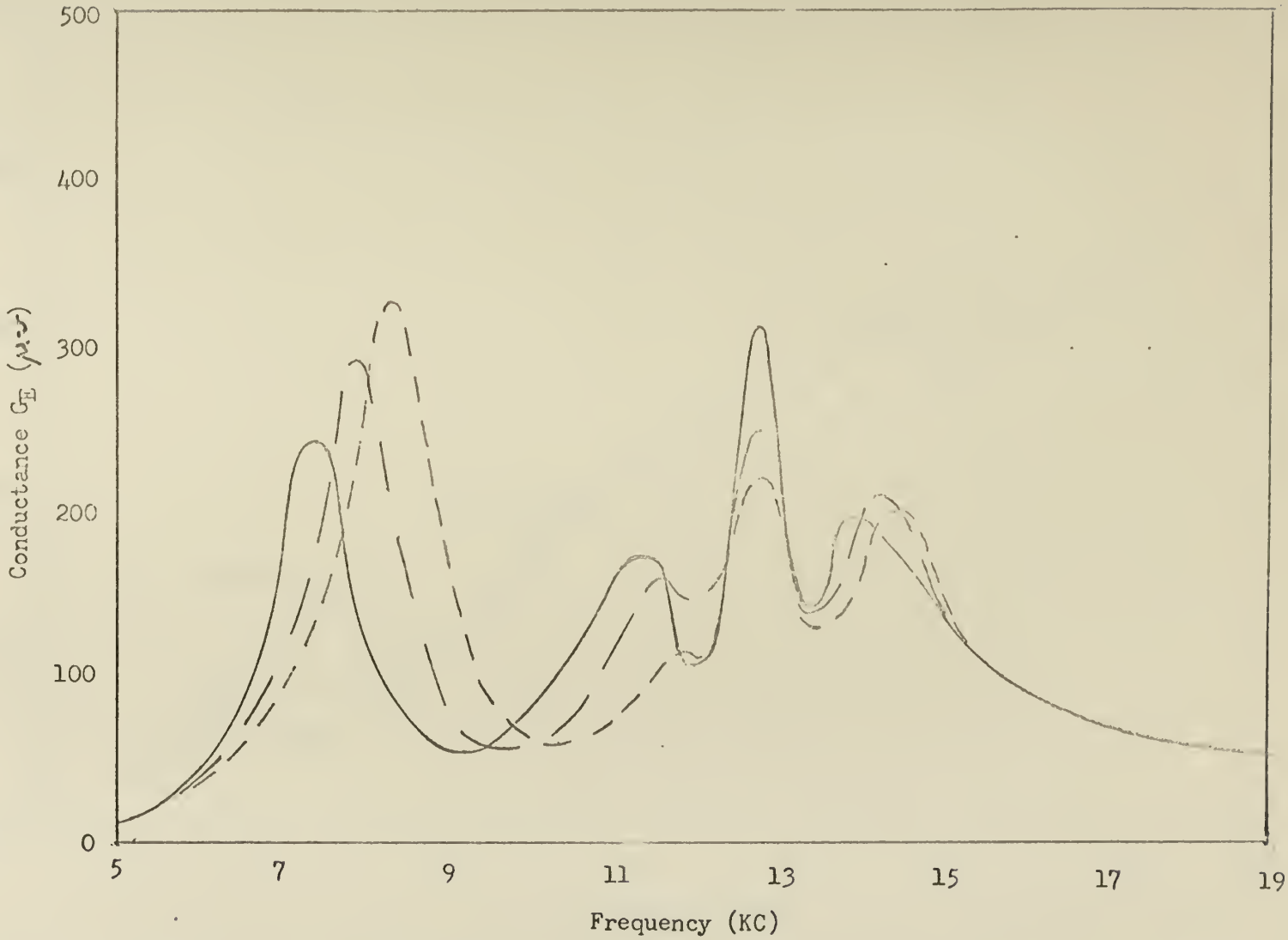

Figure 5.6 Plot of Conductance (G_E) Versus Frequency of the Three Ring Variable Internal Impedance Transducer for Three Different Settings of the Variable Impedance Tube

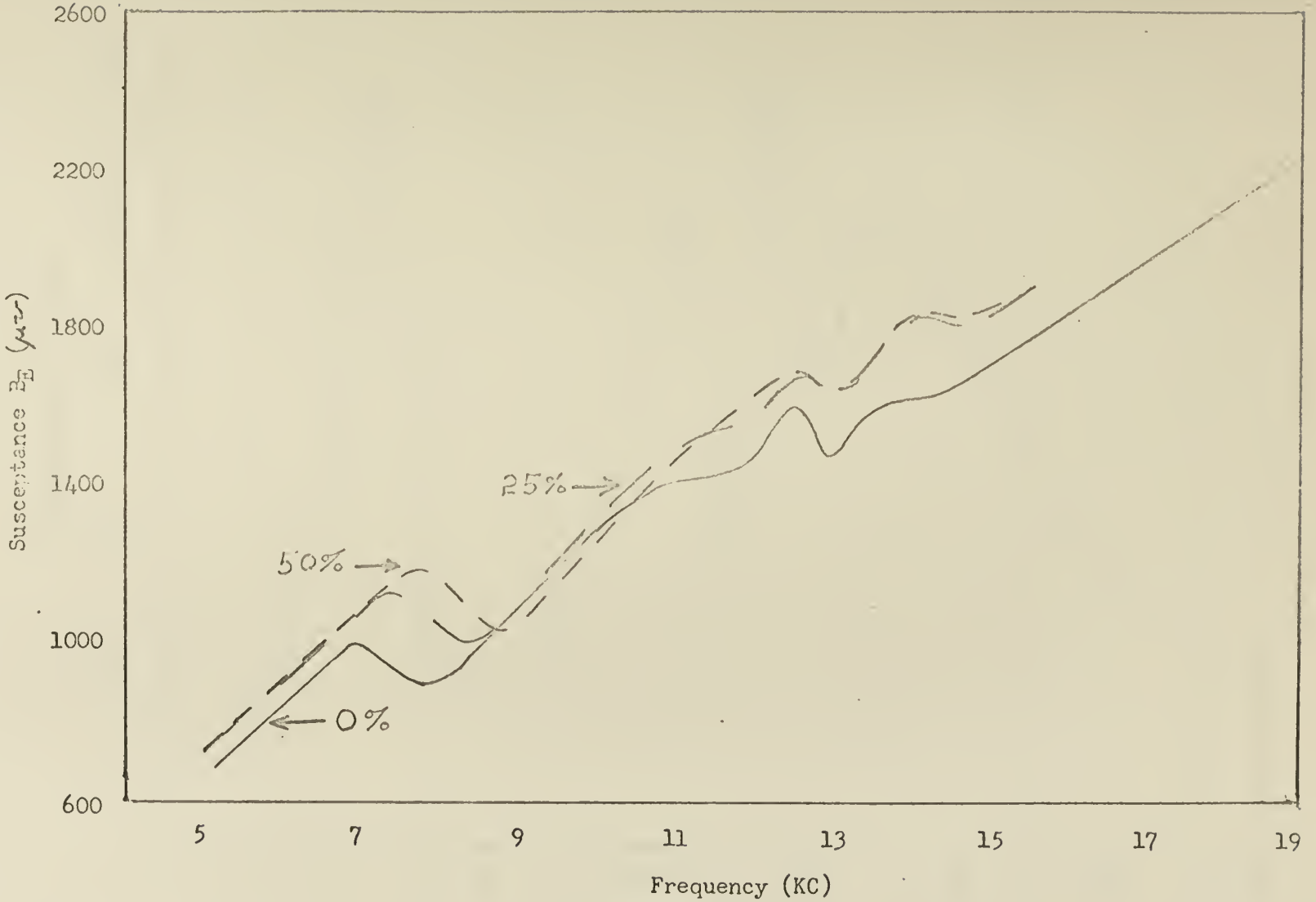

Figure 5.7 Plot of Susceptance (B_E) Versus Frequency of the Three Ring Variable Internal Impedance Transducer for Three Different Settings of the Variable Impedance Tube

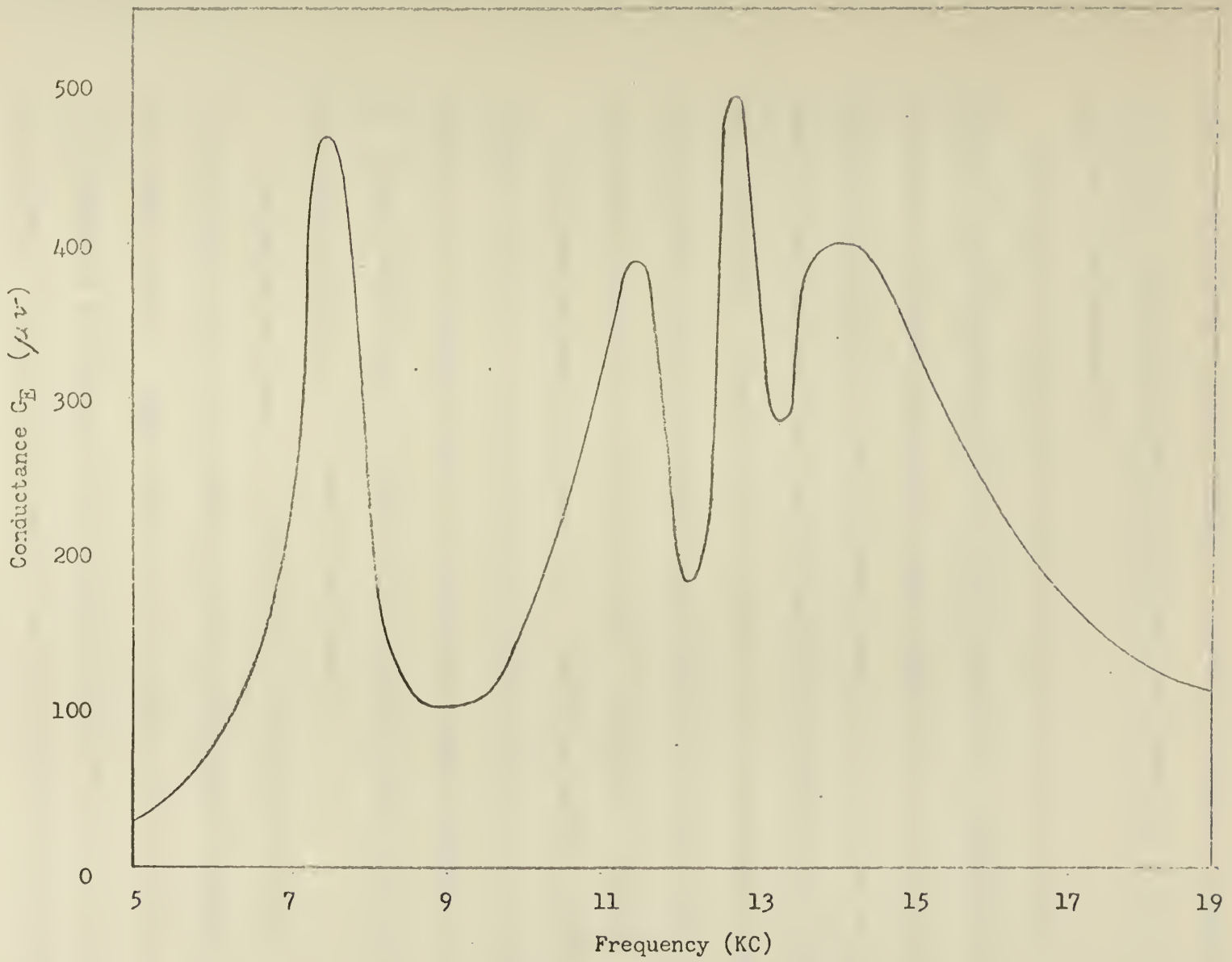

Figure 5.8 Plot of Conductance (G_E) Versus Frequency at High Power (approximately 44 watts) of the Five Ring Variable Internal Impedance Transducer with the Opening in the Variable Impedance Tube Fully Closed (Zero Percent Opening)

with the appropriate curve in Figure 5.4 reveals that there is essentially no change in the shape of the conductance curve when high power is applied to the transducer.

The graphs on Figures 5.9 and 5.10 were plotted from bridge admittance measurements made on the three ceramic ring transducer described in Section 2 with the slotted steel tubes replaced by four (3/8 inch diameter) steel support rods, while it was in water. The rods are sufficiently small,so that the transducer can be considered as having only oil inside the ceramic rings. Curves similar to those above were obtained when Scotch Calk, a putty-like material, was applied to the ends of this same transducer in an effort to damp any possible longitudinal vibrations.

The electroacoustic efficiency (η) versus percentage opening is plotted in Figure 5.11 for the two major resonant peaks of the conductance curves for the variable internal impedance transducer described in Section 2. These curves reveal the effect on the resonant peaks of varying the percentage opening in the slotted steel tubes.

The graphs on Figure 5.12 were plotted from bridge admittance measurements made on the models DX-288 and DX-239D transducers, while they were in water. These transducers are similar to the variable internal impedance transducer varying only slightly in the size of the rings, the number of rings and in the type of opening in the inner steel tube. A comparison of these transducers with the variable internal impedance transducer, Model DX-304, is made in Table 5.1.

Transducer	#Rings	Percentage opening	Type opening	d_o(in)	h(in)	t(in)
DX-304	5 & 3	variable	rectangular	6.19	2.875	.5
DX-288	6	40	circular	6.1	2.5	.5
DX-239D	3	40	circular	6.0	2.875	.375

Table 5.1 Transducer Comparison

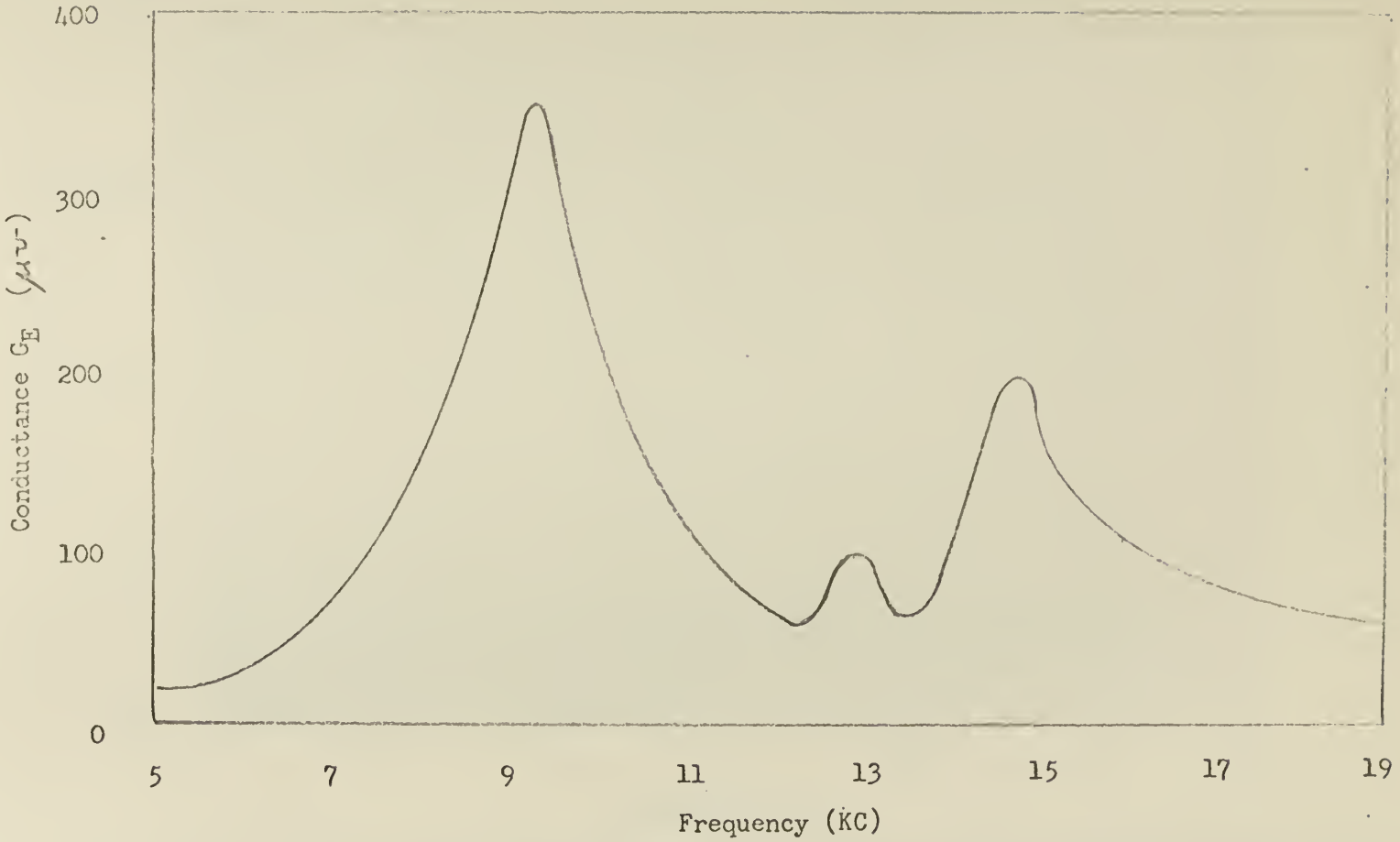

Figure 5.9 Plot of Conductance (G_E) Versus Frequency of the Three Ring Variable Internal Impedance Transducer with the Variable Impedance Tube Replaced with Four 3/8 Inch Diameter Support Rods

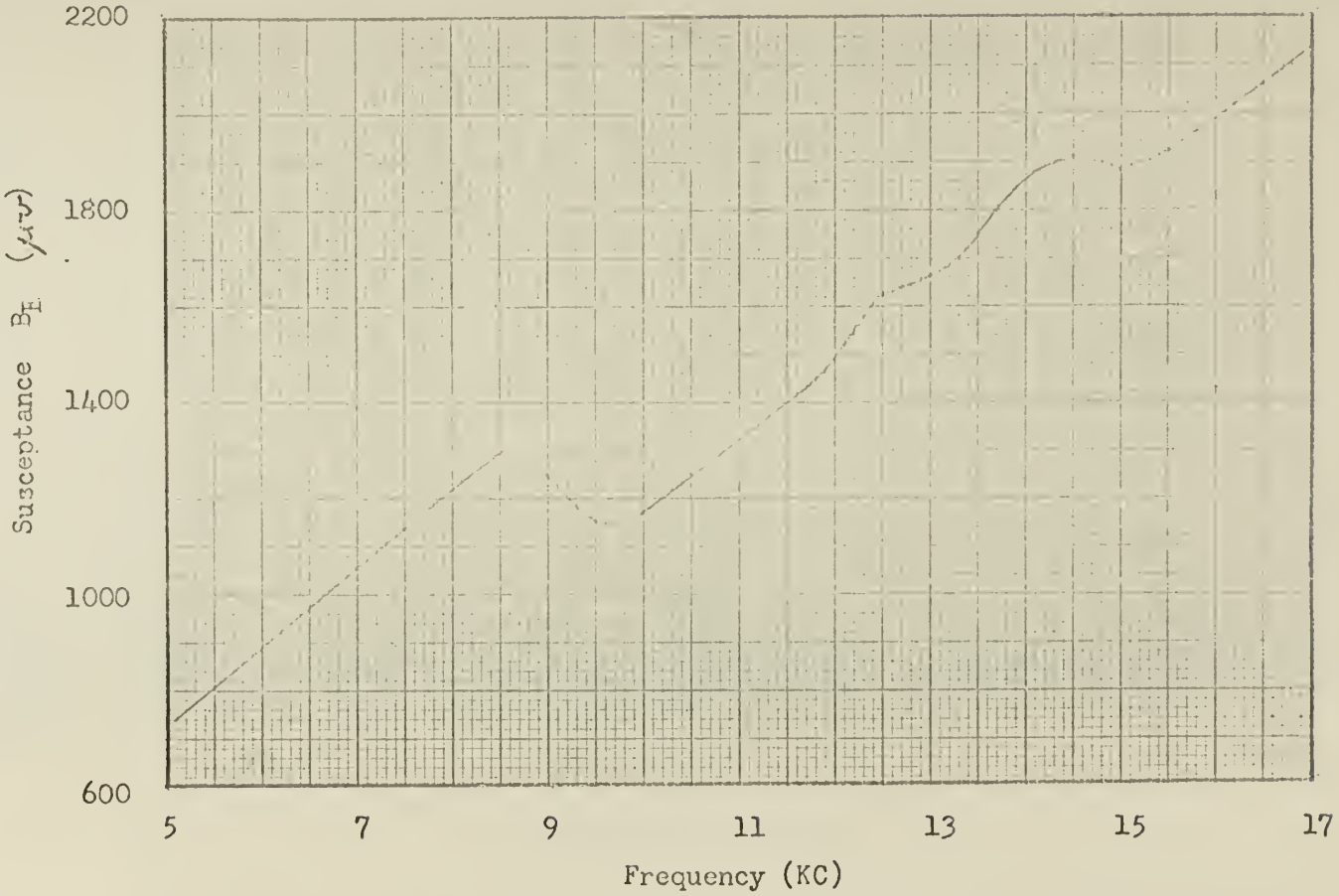

Figure 5.10 Plot of Susceptance (B_E) Versus Frequency of the Three Ring Variable Internal Impedance Transducer with the Variable Impedance Tube Replaced with Four 3/8 Inch Diameter Support Rods

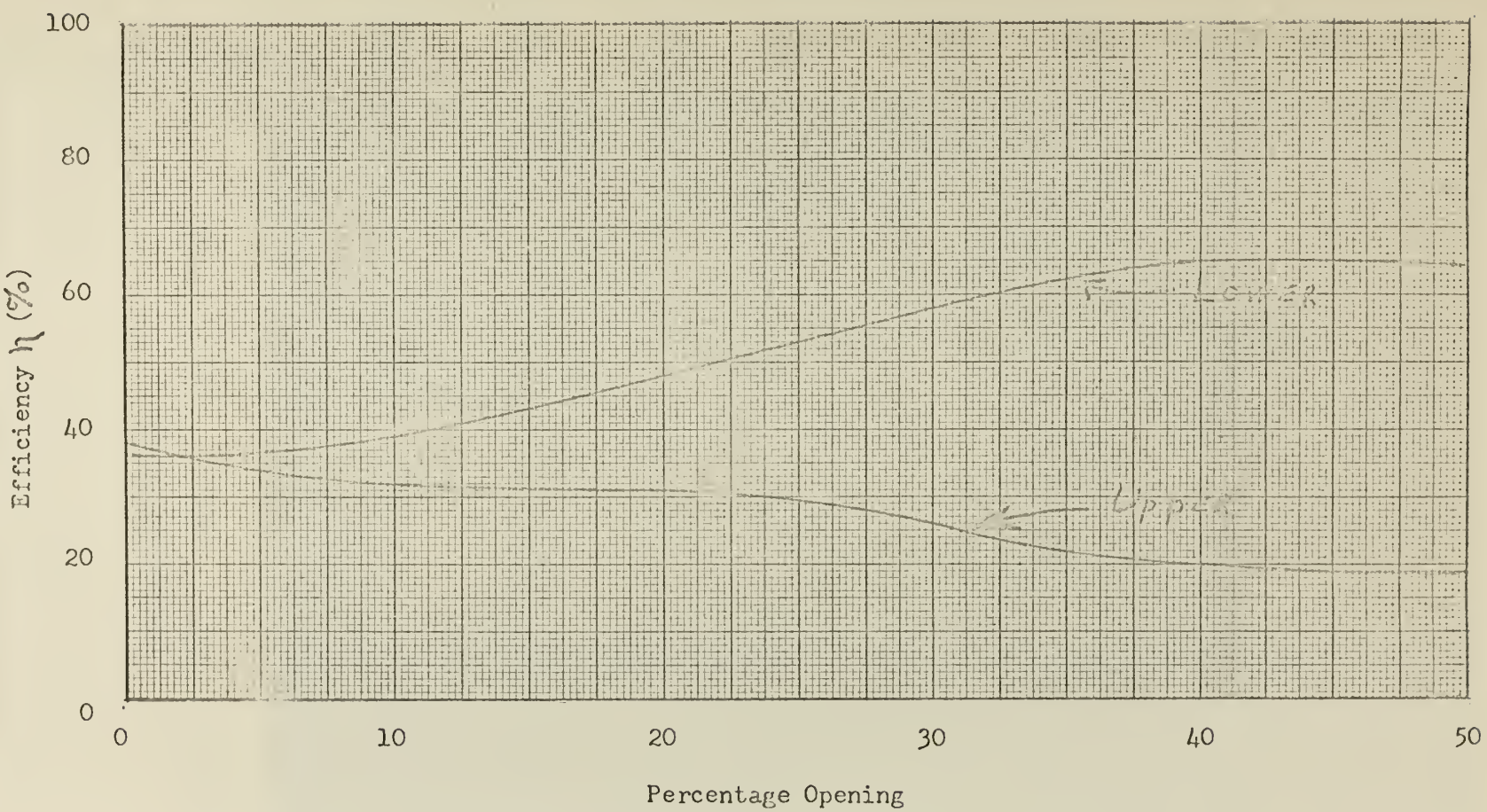

Figure 5.11 Plot of Electroacoustic Efficiency Versus Percentage Opening for the Two Major Resonances of the Variable Internal Impedance Transducer

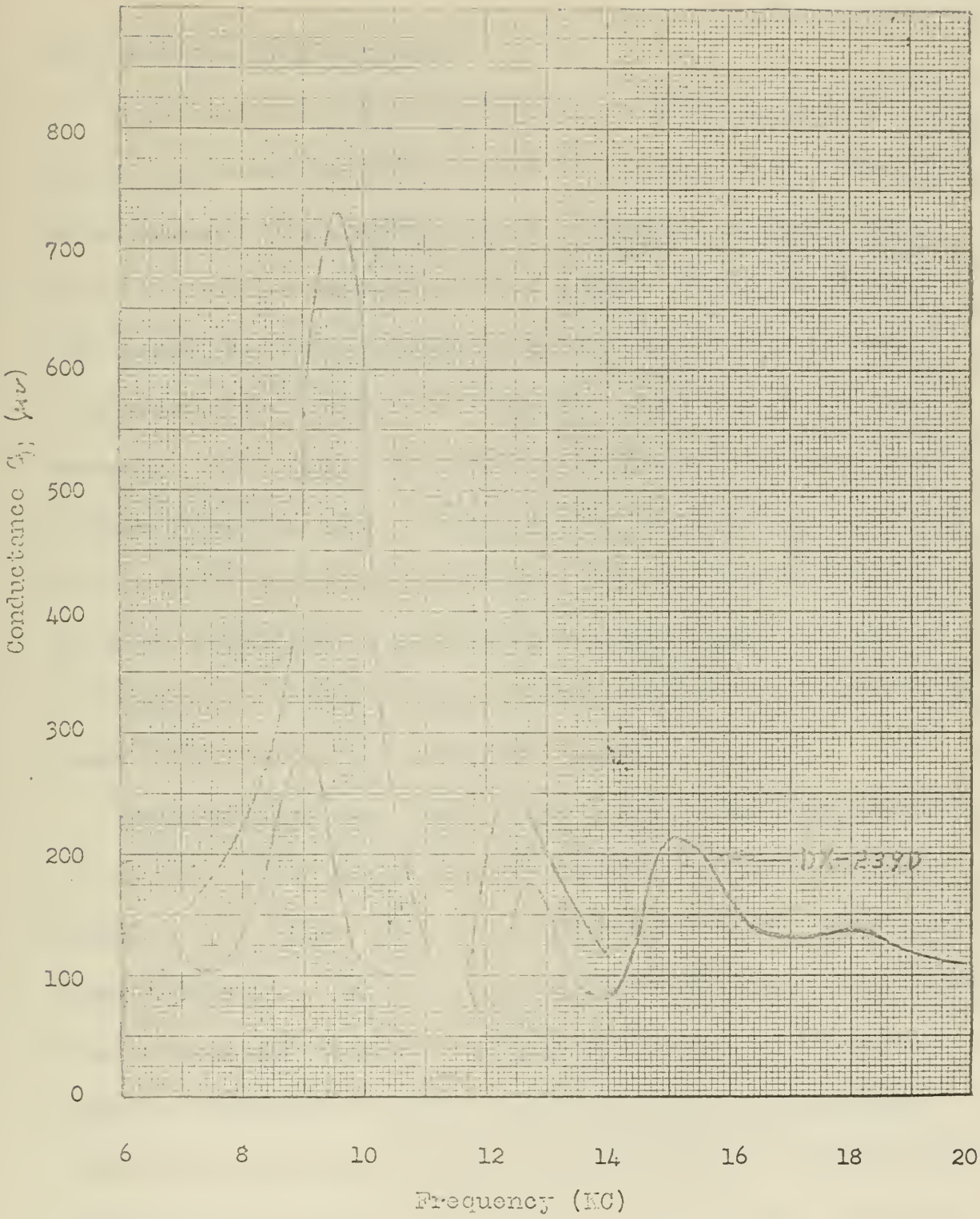

Figure 5.12

Plot of Conductance (G_p) Versus Frequency for the Models DX-288 and DX-239D Transducers

6. Discussion and Conclusions.

The placing of a stiff solid tube inside oil filled, radially vibrating, ceramic rings was expected to increase the frequency of the fundamental radial resonance of the system because of the added stiffness provided by the tube and the reduction of the oil volume. It was also expected that opening the rectangular slots in the stiff tube would be equivalent to decreasing the diameter of the stiff tube, which would decrease the frequency of the fundamental radial resonance established by the initial addition of the solid tube. A 100 percent opening in the tube would thus be essentially equivalent to removing the stiff tube from the transducer. The above expectations concerning the variable impedance transducer were based on the theory developed in Section 3 and the work done by Robey[7] and Zilinskas[8] on free flooded, vibrating, cylinders.

The experimental data for the case of a stiff-walled tube inserted in the oil filled interior agrees quite well with the expectation of a major resonance at 12.75KC. What was not expected, however, was the continued existence of a major resonance at a lower frequency, about 7.5KC, which must be associated with the fundamental radial resonance of the transducer without the stiff tube. The addition of the tube apparently caused this resonance to occur at a lower frequency and to reduce the conductance at resonance. This behaviour of the transducer can be explained as follows. First of all, the tube is not perfectly rigid. That is, waves may propagate through the walls of the tube into the enclosed oil.

Secondly, the tubes add mass to the system, resulting in a small decrease in resonance. Thirdly, the seal between the tubes may not be perfect when the slots are closed, resulting in some leakage, which would add inertance to the system and lower the resonant frequency.

The two minor resonances observed in the experimental data agree with the expectation of minor resonances around 14.6 and 15.8KC. Even though the viscous losses are small inside the oil filled rings, they cause the internal reactance curve to pass through zero between 14 and 15KC, instead of increasing to infinity. The result of this action is to create the resonance around 14.6KC shown in Figures 5.1 and 5.2 by the dashed portion of curve A. The larger the viscous losses, the lower will be the resonant frequencies of the two minor resonances. The experimental data revealed the presence of the two minor resonances for the two conditions of the transducer, with and without the stiff walled tube. The minor resonance occuring at 12.95KC for the first condition is assumed to be the same minor resonance occuring around 11.5KC for the second condition. This assumption is based on the observation of the changes in the resonant peaks occuring around 11.5KC for the second condition shown in Figures 5.4 and 5.6, as the percentage opening in the stiff tube was varied. The minor resonance at 14.8KC for the first condition is the same resonance occuring around 14.25KC for the second condition.

Various tests were made and other work was consulted to insure that these minor resonances were the ones predicted by theory as resulting from

the reactance presented to the inside of the vibrating rings by the oil fill and not by some other means. Removing the slotted tubes, changing the number of rings, increasing the power to the transducer, and applying a viscous damping compound on the transducer end plates caused no appreciable effect on these minor resonances. A study of Merriweather's report[9] revealed that minor resonances occured when the pressure release material was removed from the free flooded, radially vibrating, ceramic ring. Measurements made on similar oil filled transducers, devoid of all forms of pressure release, revealed the presence of minor resonances. Finally, unreported work accomplished by Dr. Leon Camp on free flooded, radially vibrating rings devoid of all forms of pressure release was consulted. It was revealed that the height(h) of the rings and the spacing of the rings are extremely critical with respect to the build up of minor resonances resulting from the fluid fill.

Observation of the curves for electroacoustic efficiency of the two major peaks, created by the presence of the stiff tube, shown in Figure 5.11 reveals that the efficiency of the lower major resonance predominates over that of the upper major resonance, once the slots in the tube are opened. The lower major resonance increases to 65 percent efficiency at 40 percent opening and then remains constant. The upper major resonance decreases to 19 percent efficiency at 45 percent opening and then remains constant. The above behaviour is in good agreement with the admittance measurements, where the lower major resonance becomes more pronounced and

the upper major resonance less pronounced as the slots in the stiff tube are opened.

7. Applications and Recommendations.

The results of this investigation have revealed some interesting possible applications for transducers of the type investigated. In addition to the prior-proven operation at great depths, there is the possibility of utilizing the transducer to operate on two different frequencies, either both sending, both receiving, or a combination of the two. The transducer can be designed to operate at different frequencies using the same size ceramic rings. Utilizing the upper resonant peak caused by the addition of the impedance tube would allow the use of greater diameter rings at higher frequencies, resulting in greater power handling capabilities of the transducer at the higher frequencies. With the proper ratio of diameter of the ceramic rings to the diameter of the stiff tube, the two major resonant peaks can be brought close together giving a broad bandwidth.

Further investigation of the effect of the oil fill and the presence of a stiff tube are needed. The proper height and separation of the rings to eliminate minor resonances should be determined. Methods should be investigated whereby the efficiency of the two major resonant peaks caused by the stiff tube might be increased, especially that of the higher major resonance. Investigation utilizing various diameter tubes instead of a variable percentage opening tube should be made. This sort of investigation would determine any problems that might be caused by viscous losses through a partially open tube and any lack of stiffness caused by holes cut in the tube.

BIBLIOGRAPHY

1. J. E. Martin, Design of Ceramic Cylindrical Vibrators for Sonar Transducers, Bendix-Pacific Division Report No. 8920R43, 1963.

2. T. F. Hueter and R. H. Bolt, Sonics, John Wiley and Sons, Inc., 1955.

3. W. P. Mason, Electromechanical Transducers and Wave Filters, D. Van Nostrand Company, Inc., 1958.

4. J. L. Synge and B. A. Griffith, Principles of Mechanics, McGraw-Hill Book Company, Inc., 1949.

5. L. E. Kinsler and A. R. Frey, Fundamentals of Acoustics, John Wiley and Sons, Inc., 1962.

6. U. S. National Defense Research Committee, The Design and Construction of Magnetostriction Transducers, Columbia University Press, 1946.

7. D. H. Robey, On the Contribution of a Contained Viscous Liquid to the Acoustic Impedance of a Radially Vibrating Tube, J.A.S.A., 1, pp. 22-25, Jan., 1955.

8. G. J. Zilinskas, Internal Radiation Impedance on a Liquid Filled Ceramic Cylinder, Bendix-Pacific Division Report No. 8920R44, 1963.

9. A. S. Merriweather, The Modes of Vibration in Water of Ferroelectric Cylindrical Tubes Devoid of All Forms of Pressure Release, N.E.L. Technical Memorandum 501, 1961.

10. G. Bordoni and W. Gross, Sound Radiation From A Finite Cylinder, Journal Math Phys., 27, pp. 241-252, Jan., 1949.

11. E. R. Kaiser, Acoustical Vibrations, J.A.S.A., 4 pp. 617-623, July, 1953.

12. R. A. Langevin, Electro-Acoustic Sensitivity of Cylindrical Ceramic Tubes, J.A.S.A., 3, pp. 421-427, May, 1954.

13. R. B. Lindsay, Mechanical Radiation, McGraw-Hill Book Company, Inc., 1960.

14. P. M. Morse, Vibration and Sound, McGraw-Hill Book, Co., Inc., 1948.

APPENDIX I

CLAMPED CAPACITANCE AND ELECTROMECHANICAL CONVERSION FACTOR

The values of clamped capacitance (C_o) and electromechanical conversion factor (ϕ^2) found in the equivalent circuit of Section 3 can be found from measurements made on the ceramic in air. The relations for relating C_o and ϕ^2 to the measurements made in air will be developed.

The basic equations for thickness (33) vibrators developed by Mason[3] will be assumed to apply to the tangentially (33) polarized cylindrical vibrators. This assumption is based on the similarities of the stress - strain relations for incremental segments of cylindrical vibrators and thickness vibrators. Modifying Mason's equations for thickness vibrators with the dimensions for the tangentially polarized cylinders gives the following equations:

$$C_o = N\left(\frac{N K_o h t}{4\pi^2 d_m}\right) \tag{I.1}$$

$$k_{33}^2 = \frac{d_{33}^2 K_o}{4\pi Y_{33}} \tag{I.2}$$

$$Y_o = \left(1 - \frac{8}{\pi^2} k_{33}^2\right) Y_{33} \tag{I.3}$$

$$\phi^2 = \frac{k_{33}^2 K_o Y_{33}}{4\pi} \left[\frac{N h t}{\pi d_m}\right]^2 \qquad \text{(I.4)}$$

The clamped capacitance (C_o) can be obtained as a function of the electromechanical coupling factor (k_{33}) and measured capacitance of the ceramic far below resonance (C_B). Consider the equivalent circuit for the ceramic cylinder in air as shown in Figure I.1:

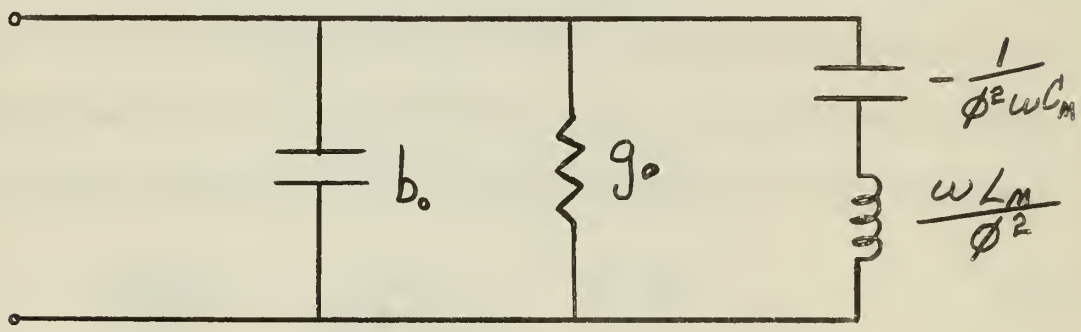

Figure I.1 Equivalent Circuit In Air

where

$$C_m = \frac{1}{K} = \frac{\pi d_m}{Y_o h t} \qquad \text{(I.5)}$$

and

$$L_M = \frac{M_o}{4\pi^2} \qquad \text{(I.6)}$$

The value of capacitance C_B measured far below resonance where L_M can be neglected is given by the following expression:

$$C_B = C_o + \phi^2 C_M \qquad \text{(I.7)}$$

Substituting Equations I.1, I.3, I.4, and I.5 into Equation I.7 gives:

$$C_B = C_o + C_o \left(\frac{k_{33}^2}{1 - \frac{8}{\pi^2} k_{33}^2} \right) \tag{I.8}$$

Solving Equation I.8 for C_o results in:

$$C_o = \frac{C_B}{1 + \left(\frac{k_{33}^2}{1 - \frac{8}{\pi^2} k_{33}^2} \right)} \tag{I.9}$$

The development of the coefficient of electromechanical coupling (k_{33}) in terms of air measurements requires a look at the resonance and anti-resonance of the ceramic cylinder in air. At mechanical resonance the electrical reactance of the motional admittance is zero[5]; therefore,

$$\frac{\omega L_M}{\phi^2} - \frac{1}{\phi^2 \omega C_M} = 0 \tag{I.10}$$

Solving for the resonant frequency in air (f_{RA}) gives:

$$f_{RA} = \frac{1}{2\pi \sqrt{L_M C_M}} \tag{I.11}$$

At anti-resonance the susceptance of the series-parallel circuit is zero[5]; therefore,

$$\omega C_o + \frac{1}{\frac{\omega L_M}{\phi^2} - \frac{1}{\phi^2 \omega C_M}} = 0 \tag{I.12}$$

Solving for the anti-resonant frequency in air gives:

$$f_{AA} = \frac{1}{2\pi} \sqrt{\frac{\frac{\phi^2 C_M}{C_o} + 1}{L_M C_M}} \tag{I.13}$$

Taking the ratio of the squares of Equations I.11 and I.13 gives:

$$\frac{f_{AA}^2}{f_{RA}^2} = \frac{\phi^2 C_M}{C_o} + 1 \qquad \text{(I.14)}$$

Substituting the value for $\phi^2 C_M$ from Equations I.7 and I.8 gives:

$$\frac{f_{AA}^2}{f_{RA}^2} = \frac{k_{33}^2}{1 - \frac{8}{\pi^2} k_{33}^2} + 1 \qquad \text{(I.15)}$$

Solving for k_{33} in Equation I.15 results in:

$$k_{33} = \sqrt{\frac{\frac{f_{AA}^2 - f_{RA}^2}{f_{RA}^2}}{1 + \frac{8}{\pi^2}\left(\frac{f_{AA}^2 - f_{RA}^2}{f_{RA}^2}\right)^2}} \qquad \text{(I.16)}$$

The electromechanical conversion factor (ϕ^2) can be related to quantities which can be measured in air. Solving Equation I.14 for ϕ^2 gives:

$$\phi^2 = \left(\frac{f_{AA}^2}{f_{RA}^2} - 1\right)\frac{C_o}{C_M} \qquad \text{(I.17)}$$

Substituting Equation 3.23 and I.5 for C_M in Equation I.17 results in

$$\phi^2 = \left(\frac{f_{AA}^2 - f_{RA}^2}{f_{RA}}\right) C_o Z_o \qquad \text{(I.18)}$$

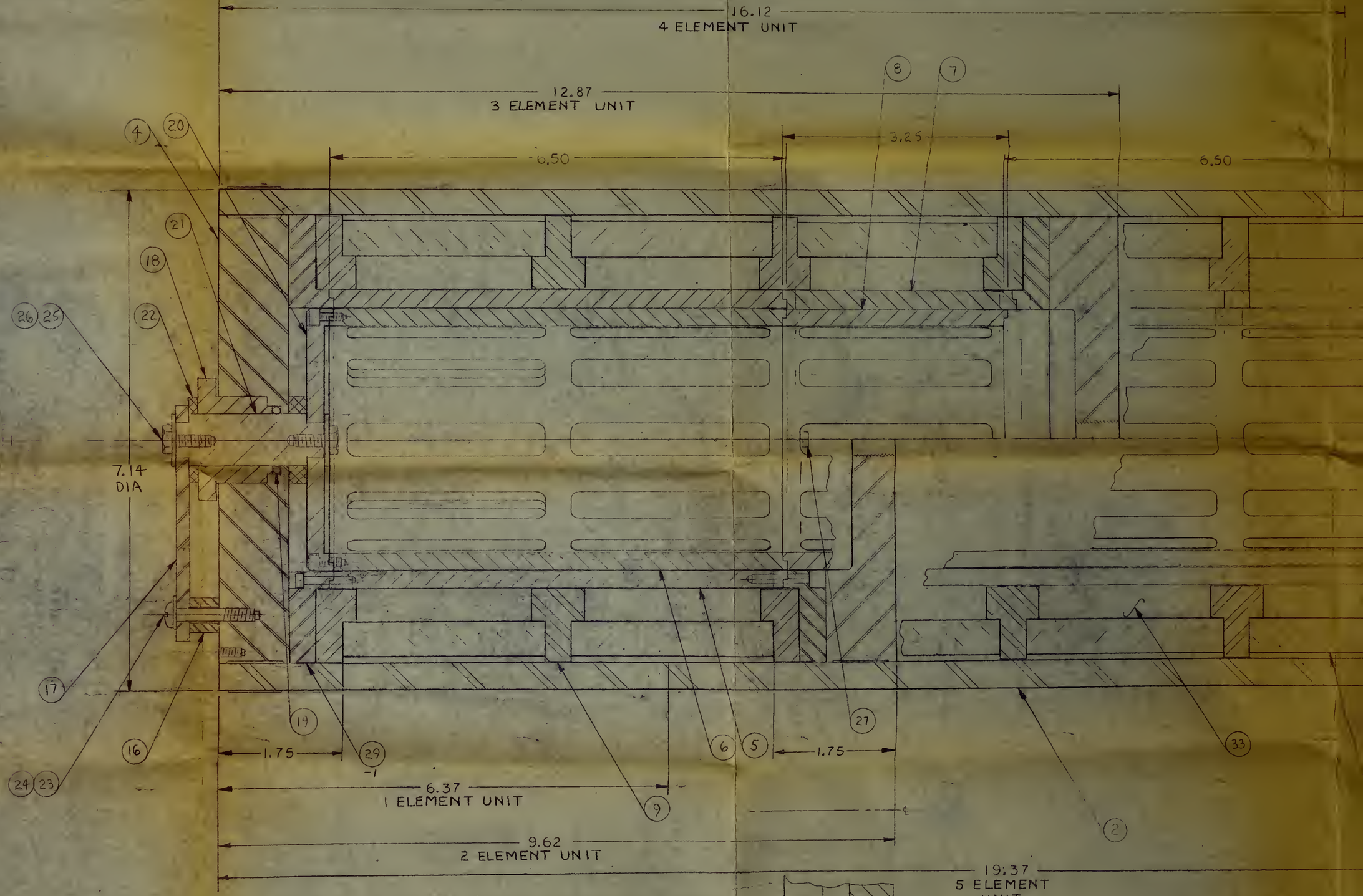
16.12
4 ELEMENT UNIT
12.87
3 ELEMENT UNIT
6.50
3.25
6.50
7.14
DIA
1.75
1.75
6.37
1 ELEMENT UNIT
9.62
2 ELEMENT UNIT
19.37
5 ELEMENT
UNIT
4
20
21
18
26
25
22
8
7
17
16
24
23
19
29
-1
6
5
27
33
9
2

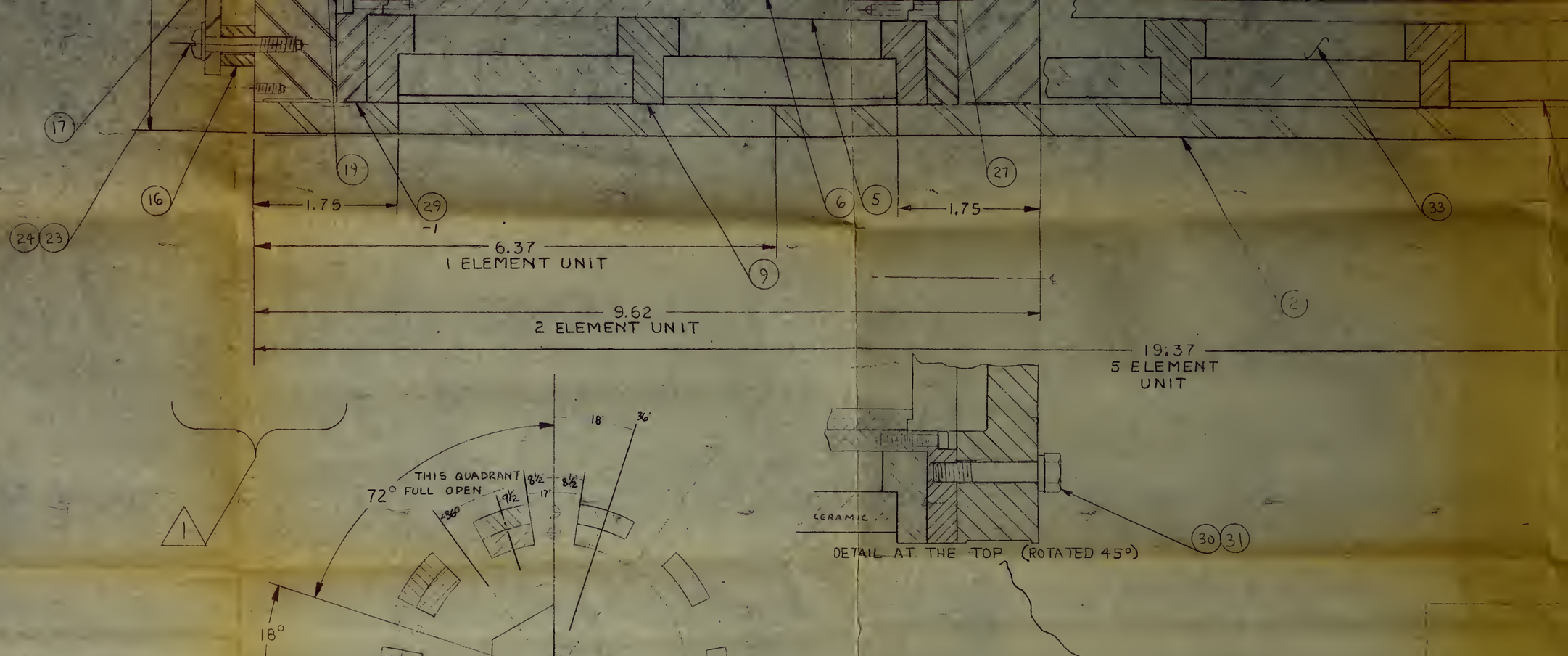

VARIABLE OPENING
LAY OUT

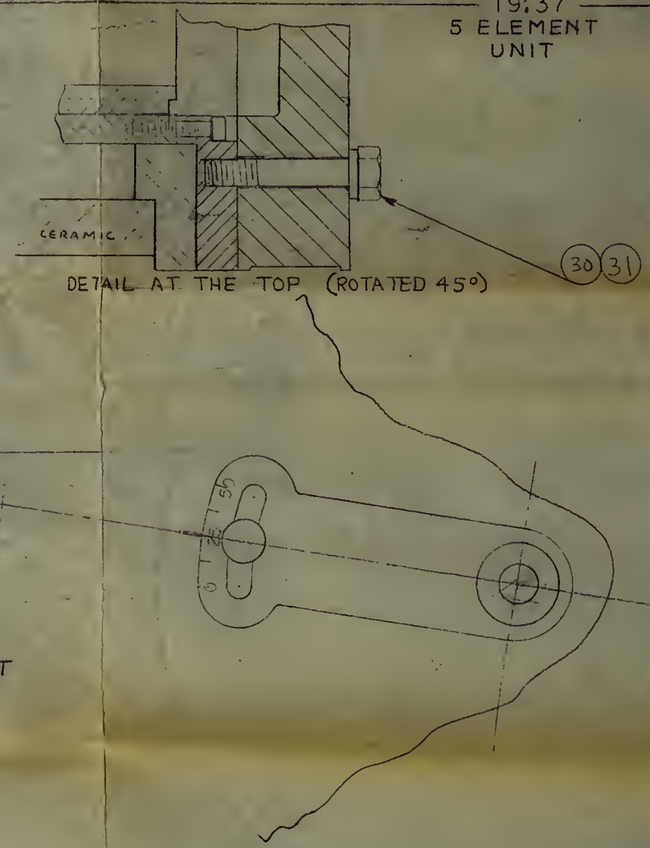

33	AS REQ	
31	8	30
30	8	MS3
29	1	31

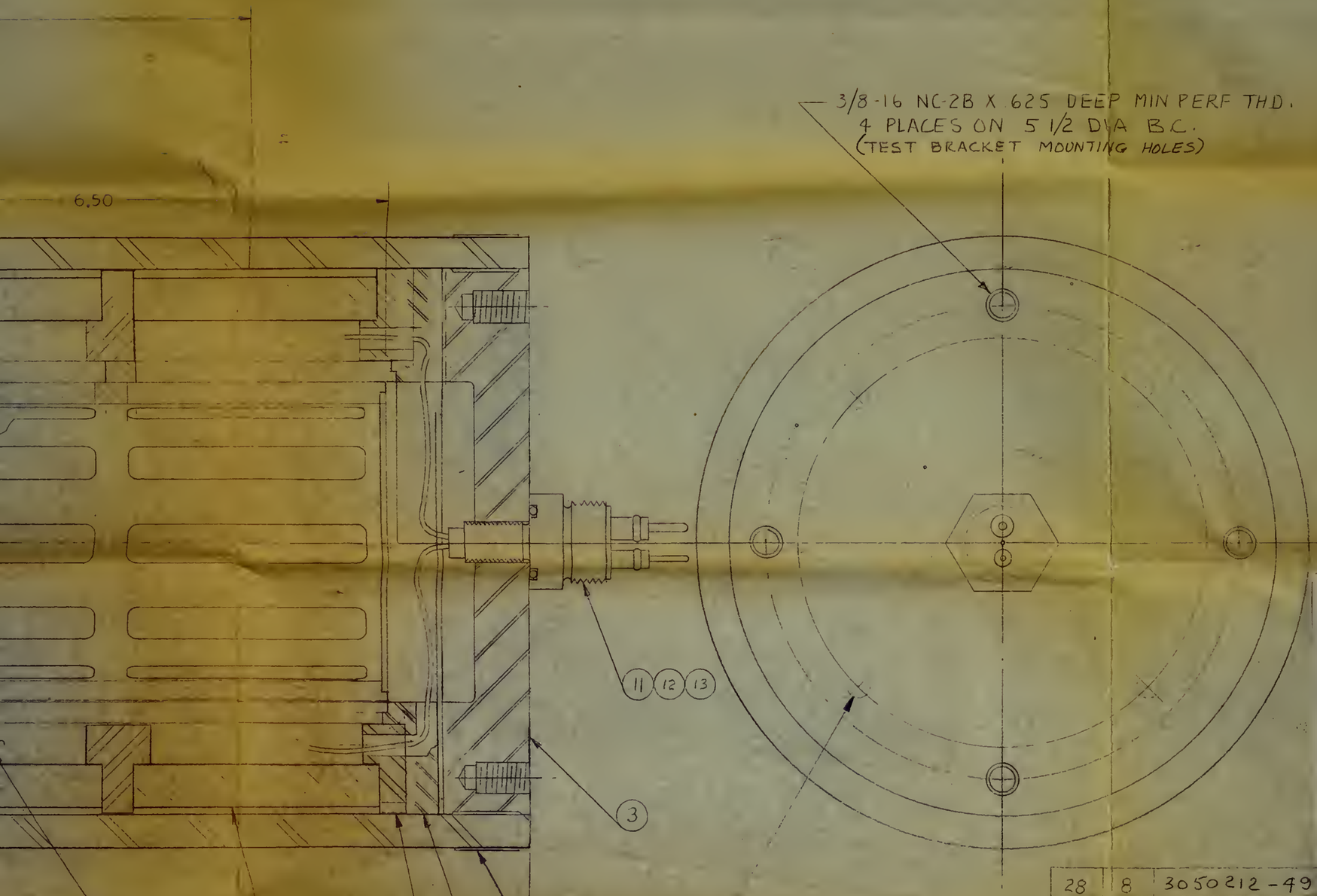

Figure 2.3 Layout of the Variable Internal Impedance Transducer

28	8	3050212-49	SCREW-SOC HD CAP	6-32 X 3/4 HI STRENGTH CRS
27	20	3050212-46	SCREW-SOC HD CAP	6-32 X 3/8 HI STRENGTH CRS
26	2		WASHER	#10 STAINLESS 3/4 OD
25	2	MS35229-65	BOLT	10-32 X 3/4 BRASS
24	1	MS15795-609	WASHER	#10 STAINLESS
23	1	MS35229-67	SCREW	10-32 X 1 PAN HD BRASS
22	2	3143598	WASHER	TEFLON
21	1	3143548	SHAFT	STAINLESS
20	1	3143596	COVER-PLATE	3/8 CR STEEL

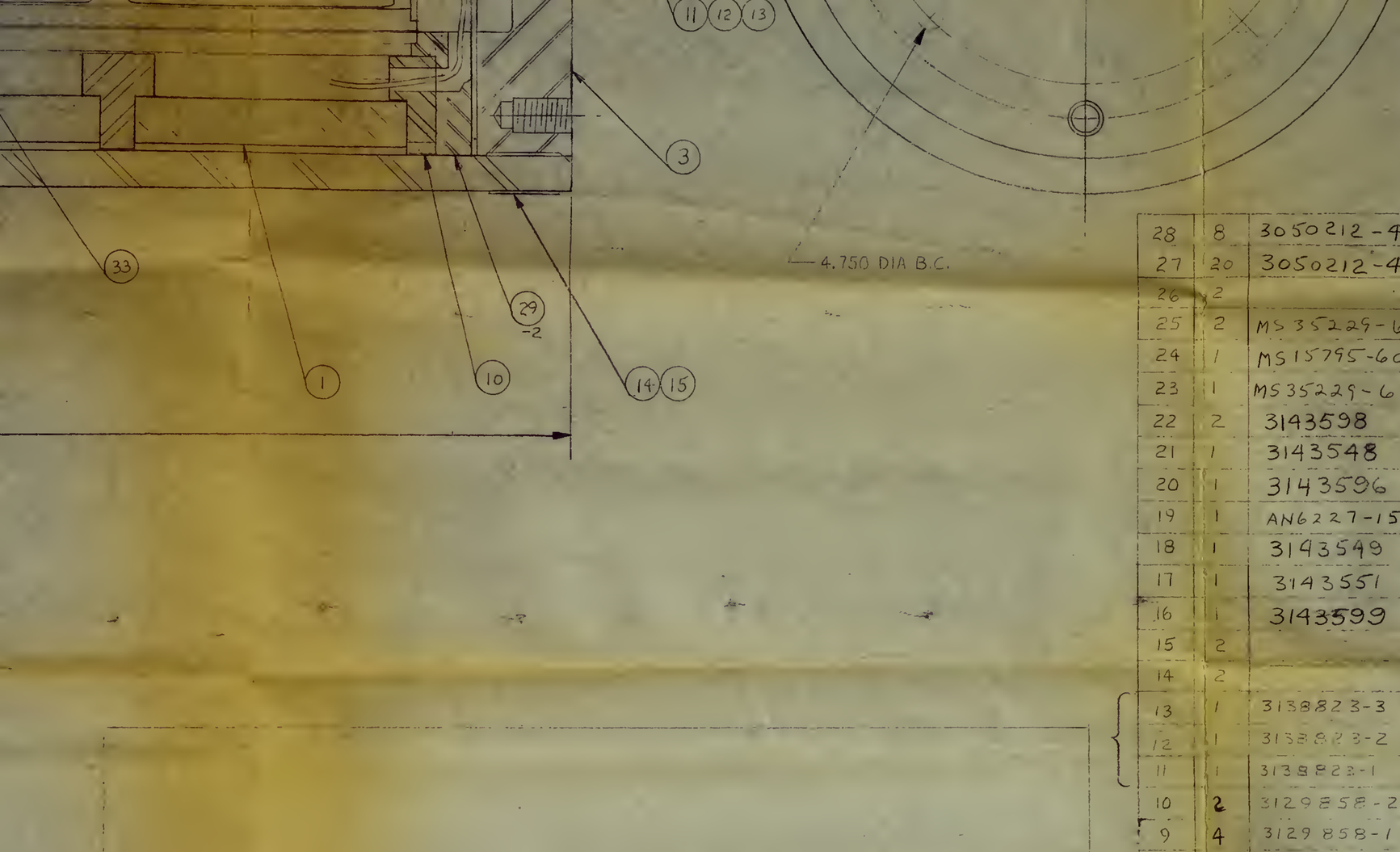

Figure 2.3 Layout of the Variable Internal Impedance Transducer

ITEM NO.	QTY REQD	PART OR IDENTIFYING NO.	NOMENCLATURE OR DESCRIPTION	MATERIAL SIZE, DESCRIPTION & SPECIFICATION
28	8	3050212-49	SCREW-SOC HD CAP	6-32 X 3/4 HI STRENGTH CRS
27	20	3050212-46	SCREW-SOC HD CAP	6-32 X 3/8 HI STRENGTH CRS
26	2		WASHER	#10 STAINLESS 3/4 OD
25	2	MS35229-65	BOLT	10-32 X 3/4 BRASS
24	1	MS15795-609	WASHER	#10 STAINLESS
23	1	MS35229-67	SCREW	10-32 X 1 PAN HD BRASS
22	2	3143598	WASHER	TEFLON
21	1	3143548	SHAFT	STAINLESS
20	1	3143596	COVER-PLATE	3/8 CR STEEL
19	1	AN6227-15	O RING	NEOPRENE
18	1	3143549	NUT	BRASS
17	1	3143551	ARM	3/16 STAINLESS
16	1	3143599	POST TUBE	BRASS
15	2		CLIP	STAINLESS
14	2		BAND	.020 X 3/4 STAINLESS
13	1	3138823-3	NUT	MECCA NOT SHOWN
12	1	3138823-2	CONNECTOR	MECCA CABLE 31 FT LG NOT SHOWN
11	1	3138823-1	RECEPTACLE	MECCA
10	2	3129858-2	SPACER-ELEMENT	QUANTITY IS FOR 5 DIFFERENT UNITS
9	4	3129858-1	SPACER-ELEMENT	MODIFY OD TO FIT
8	1	3143547	CAGE -SHORT INNER	CR STEEL 1/4 WALL
7	1	3143545	CAGE -SHORT OUTER	CR STEEL 1/4 WALL
6	2	3143546	CAGE -LONG INNER	CR STEEL 1/4 WALL 3.75 OD X 3.250 ID
5	2	3143544	CAGE -LONG OUTER	CR STEEL 1/4 WALL 4.25 OD X 3.750 ID
4	1	3143550	BODY - LOWER	CR STEEL ZINC PLATED
3	1	3143552	BODY - UPPER	CR STEEL ZINC PLATED
2	1	3142050-4	BOOT	26.00 X 6.38 X .38 (CUT TO LENGTH AS REQ)
1	5	3132873	CERAMIC	2.875 Lg X 6.187 OD X 5.187 ID.

LIST OF MATERIAL OR PARTS LIST

ITEM NO.	QTY REQD	PART OR IDENTIFYING NO.	NOMENCLATURE OR DESCRIPTION	MATERIAL SIZE, DESCRIPTION & SPECIFICATION
33	AS REQ		OIL	CASTOR DB
31	8	3068569-36	WASHER SEAL	PARKER SEALS (# 1/4)
30	8	MS35309-11	BOLT HEX HEAD	1/4-20 X 1 3/8 BRASS
29	1	3143543 -1 -2	ADAPTER PLATE	CR STEEL

FOR IN PLANT USE ONLY
NOT TO BE SOLD

3143464	3143464		
NEXT ASSY	USED ON	NEXT ASSY	FINAL ASSY
APPLICATION		QTY REQD	

UNLESS OTHERWISE SPECIFIED

- INTERPRET DRAWING IN ACCORDANCE WITH MIL-D-70327 INCLUDING APPLICABLE DOCUMENTS REFERENCED THEREIN.
- DIMENSIONS TO BE MET _____ PROTECTIVE COATING.
- REMOVE ALL BURRS, BREAK SHARP EDGES _____ MAX.
- BEND RADII AND RELIEF RADII 2 TIMES THICKNESS.

UNLESS OTHERWISE SPECIFIED
DIMENSIONS ARE IN INCHES
TOLERANCES ON
DECIMALS: .X ± .1, .XX ± .03, .XXX ± .010
ANGLES: ± 0° 30'

DO NOT SCALE THIS DRAWING
PROJECT OR CONTRACT NO.

DRAWN		
CHECK		
ENGR	H. Lewis	10-8-62
GROUP LEADER		
PROJ ENGR	J Merrill	11-27-62

APPROVED

THE Bendix CORPORATION BENDIX-PACIFIC DIVISION NORTH HOLLYWOOD, CALIFORNIA

NPR STUDY
DX304

CODE IDENT NO 77068 | SIZE E | 3143464

ACOUSTIC DESIGN CHECK
CONSULTANT J.t. martin DATE 11/27/62
PROJECT ENGINEER DATE
APPROVED FOR:

PRODUCT NO.